

**Copper and Nitrogen co-doped TiO₂/ Graphene
Oxide Nanocomposites for Photocatalytic
Degradation of Methyl Orange**



**Name: Komal Javed
Reg. # 00000117027**

**This thesis is submitted as a partial fulfillment of the
requirements for the degree of
Master of Science in
Chemistry**

**Supervised by: Prof. Dr. Habib Nasir
Department of Chemistry
School of Natural Sciences (SNS)
National University of Sciences and Technology (NUST)
H-12, Islamabad, Pakistan**

2017

National University of Sciences & Technology**MS THESIS WORK**

We hereby recommend that the dissertation prepared under our supervision by: KOMAL JAVED, Regn No. 00000117027 Titled: Copper and Nitrogen co-doped TiO₂/ Graphene Oxide Nanocomposites for Photocatalytic Degradation of Methyl Orange be accepted in partial fulfillment of the requirements for the award of **MS** degree.

Examination Committee Members1. Name: DR. ZAHIDA MALIKSignature: 2. Name: DR. FAROHA LIAQATSignature: 

3. Name: _____

Signature: _____

External Examiner: DR. TARIQ MAHMOODSignature: Supervisor's Name: PROF. HABIB NASIRSignature: 


Head of Department


18-12-17
Date


COUNTERSIGNEDDate: 18-12-17



Dean/Principal

THESIS ACCEPTANCE CERTIFICATE

Certified that final copy of MS thesis written by **Ms. Komal Javed**, (Registration No. **00000117027**), of **School of Natural Sciences** has been vetted by undersigned, found complete in all respects as per NUST statutes/regulations, is free of plagiarism, errors, and mistakes and is accepted as partial fulfillment for award of MS/M.Phil degree. It is further certified that necessary amendments as pointed out by GEC members and external examiner of the scholar have also been incorporated in the said thesis.

Signature: _____  _____
Name of Supervisor: Prof. Habib Nasir
Date: _____ 18-12-17 _____

Signature (HoD): _____  _____
Date: _____ 18-12-17 _____

Signature (Dean/Principal): _____  _____
Date: _____ 18-12-17 _____

*In the name of ALLAH, the
Gracious, the Merciful*

Dedicated to

*My beloved parents Ch. Javed Iqbal, Zahida
Javed and my siblings Fahad, Zaryab, Bilal
and Rameen*

Acknowledgements

*First of all, I would like to thank **Allah Almighty**, who has given me the ability, courage and His blessings to complete this thesis. He gave me strength and right path throughout my research work.*

*My special and sincere thanks to principal of SNS and my supportive supervisor, **Prof. Dr. Habib Nasir** for providing me the most peaceful environment to work and guiding me throughout my research work. A special thanks to my guidance and evaluation committee members, **Dr. Zahida Malik** and **Dr. Faroha Liaquat**, for their valuable guidance, suggestions and encouragement. I am grateful especially to **School of Natural Sciences, NUST** for providing me all the facilities and a platform to work. I greatly acknowledge the facilities and technical support provided by other schools of NUST like **IESE, SCME, SMME** and other institutes like **National Centre for Physics and Quaid-e-Azam University, Islamabad**.*

*Finally, I would like to express my gratitude to all my righteous friends **Soha Safdar, Urooj Iqbal, Fareha Gul, Rimsha Mehek, Fakhira Riaz, Aroosa Javed, Tanzeela Akram** and **Zaib-un-Nisa** for their loyal support, guidance, encouragement and prayers. I would like to thank my family members specially my dady **Ch. Javed Iqbal** and my mama **Zahida Javed** for being so supportive and loving, my brothers **Fahad Javed, Zaryab Javed, Bilal Javed** and my loving sister **Rameen Javed** for always being there and helping me whenever I needed them.*

Komal Javed

Abstract

Photocatalysis based on semiconductors is a likely approach to overcome many pollution problems and eliminate toxic organic compounds from waste-water. TiO_2 due to its unique properties is considered as a promising semiconductor. Despite its intriguing properties, TiO_2 is unable to absorb visible part of light due to which the overall photocatalytic activity is affected. In this thesis, TiO_2 nanoparticles were synthesized in its pure anatase phase using sol-gel method. To reduce the band gap, N doped TiO_2 and N and Cu co-doped TiO_2 nanoparticles with varying concentrations of Cu (0.1%, 0.5%, 1%, 2%, 3 wt %) were synthesized to obtain both non-metal and metal dopant properties. Tetra titanium iso-propoxide, urea and $\text{Cu}(\text{NO}_3)_2 \cdot 3\text{H}_2\text{O}$ were used as precursors for TiO_2 nanoparticles and N and Cu doping, respectively. The prepared catalysts were characterized using XRD, SEM, EDS, FT-IR and UV/Vis-DRS. Both crystallite size and particle size for doped catalysts were reduced as compared to pure TiO_2 nanoparticles. The degradation studies for the prepared photocatalysts were performed on methyl orange under visible light using LEDs. The kinetic studies exhibited that photocatalytic performance of 2% Cu/N co-doped TiO_2 was best amongst all prepared catalysts with an efficiency of 93%. To further improve the efficiency, nanocomposites of the as-prepared best catalyst and graphene oxide were prepared. GO nanosheets were prepared using Hummers' method by using graphite flakes as a precursor and KMnO_4 as an oxidizing agent. Incorporation of 2% Cu/N co-doped TiO_2 nanoparticles on GO sheets was done by using hydrothermal method and different percentages of GO: TiO_2 (0.5:1, 1:1 and 2:1) were prepared to study the effect of amount of GO. Degradation studies were performed on methyl orange again and the kinetic studies showed that the efficiency was increased to 96%.

Table of Contents

1 INTRODUCTION	1
1.1 Background.....	1
1.2 Photocatalyst	1
1.2.1 Mechanism of photocatalysis in TiO ₂	2
1.3 Doping	3
1.3.1 Doping with metals.....	4
1.3.2 Doping with non-metals	4
1.4 Graphene and graphene oxide	5
1.5 Graphene oxide and TiO ₂ nanocomposites.....	6
1.6 Synthesis routes for nanocomposite preparation.....	7
1.6.1 Synthesis routes for TiO ₂	7
1.6.2 Synthesis routes for graphene and graphene oxide	10
1.6.3 Synthesis routes of graphene-metal oxide nanocomposite.....	11
1.7 Dyes.....	12
1.7.1 Color of dyes	12
1.7.2 Types of dyes.....	12
1.7.3 Need for dye degradation	13
1.7.4 Methyl orange.....	13
1.7.5 Dye degradation mechanism by photocatalyst.....	14
1.8 Characterization techniques.....	15
1.8.1 Scanning electron microscopy (SEM).....	16
1.8.2 Energy dispersive X-ray spectroscopy (EDS or EDX)	17
1.8.3 X-ray diffraction (XRD).....	18
1.8.4 Fourier transform infrared spectroscopy (FTIR).....	19

1.8.5 UV-visible absorption spectroscopy.....	20
1.9 Objectives of this work.....	22
2 LITERATURE REVIEW	23
2.1 TiO ₂ nanoparticles	23
2.2 Nitrogen doped TiO ₂	25
2.3 Copper and nitrogen doped TiO ₂	27
2.4 Graphene oxide as a photocatalyst	29
2.5 Graphene oxide/ TiO ₂ nanocomposite.....	31
3 EXPERIMENTAL WORK	34
3.1 Synthesis of TiO ₂ nanoparticles	34
3.1.1 Materials and chemicals	34
3.1.2 Procedure for synthesis of TiO ₂ nanoparticles	34
3.1.3 Procedure for synthesis of nitrogen doped TiO ₂ nanoparticles	35
3.1.4 Procedure for synthesis of copper and nitrogen co-doped TiO ₂ nanoparticles	35
3.2 Synthesis of graphene oxide.....	36
3.2.1 Materials and chemicals	36
3.2.2 Procedure for graphene oxide synthesis	37
3.3 Synthesis of GO/Cu-N co-doped TiO ₂ nanocomposite.....	38
3.3.1 Chemicals and materials.....	38
3.3.2 Procedure	38
4 RESULTS AND DISCUSSION	40
4.1 Structural and morphological analysis	40
4.1.1 XRD.....	40
4.1.2 SEM.....	44
4.1.3 EDS/EDX	47

4.1.4 FT-IR	51
4.1.5 UV/visible DRS	52
4.2 Degradation studies	55
5 CONCLUSION	65
6 REFERENCES	66

List of Figures

Figure 1.1 Illustration of basic mechanism of a photocatalyst	2
Figure 1.2 Mechanism of photocatalytic phenomena of TiO ₂ . (hv ₁ : pure TiO ₂ , hv ₂ : metal-doped TiO ₂ , hv ₃ : nonmetal-doped TiO ₂)	3
Figure 1.3 Allotropic forms of carbon: (a) Diamond, (b) Graphite, (c) Lonsdaleite, (d) Fullerene, (e) Fullerite, (f) Amorphous Carbon (g) CNTs	5
Figure 1.4 Exfoliation and oxidation of graphite into single layered graphene oxide	6
Figure 1.5 Scheme of GO-TiO ₂ photocatalytic activity under UV-visible light	7
Figure 1.6 Scheme of TiO ₂ nanoparticle synthesis via sol-gel method	8
Figure 1.7 Flow sheet diagram for different synthesis routes of graphene	10
Figure 1.8 Flow chart for classification of dyes	13
Figure 1.9 (a) Yellow form of methyl orange (b) Red form of methyl orange	14
Figure 1.10 Schematic illustration of photodegradation of dye under light irradiation	14
Figure 1.11 Schematic illustration of SEM	16
Figure 1.12 Schematic illustration of EDS/EDX	17
Figure 1.13 Bragg's law of diffraction	18
Figure 1.14 Schematic illustration of FTIR spectrometer	19
Figure 1.15 Schematic illustration of UV/visible spectrometer	21
Figure 2.1 Schematic illustration of steps involved in sol-gel method	24
Figure 2.2 Schematic representation of UV and visible light absorption of N-doped TiO ₂	26
Figure 2.3 SEM image of C/N co-doped TiO ₂ nanoparticles	27
Figure 2.4 Schematic illustration of copper doped TiO ₂ based photocatalysis	29
Figure 2.5 Scheme of photocatalytic activity of N-doped TiO ₂ / GO composite	32
Figure 2.6 Schematic illustration of synthesis and photocatalysis of TiO ₂ / GO nanocomposite	33
Figure 3.1 (a) TTIP + propanol solution, (b) Drop-wise addition to H ₂ O+HNO ₃ solution	35
Figure 3.2 Schematic illustration for the preparation of Cu/N co-doped TiO ₂ nanoparticles	36
Figure 3.3 Schematic illustration of synthesis of graphene oxide	37

Figure 3.4 Prepared GO/Cu-N co-doped TiO ₂ nanocomposites	38
Figure 4.1 XRD peaks of prepared nanoparticles showing: (a) Pure TiO ₂ (b) N- TiO ₂ (c) 0.1% Cu-NT (d) 0.5% Cu-NT (e) 1% Cu-NT (f) 2% Cu-NT (g) 3% Cu-NT	40
Figure 4.2 XRD peaks of prepared nanocomposites showing: (a) 0.5:1 GO-T (b) 1:1 GO-T (c) 2:1 GO-T	41
Figure 4.3 SEM images: (a) Pure TiO ₂ (b) N- TiO ₂ (c) 0.1% Cu-NT (d) 0.5% Cu-NT (e) 1% Cu-NT (f) 2% Cu-NT (g) 3% Cu-NT	45
Figure 4.4 SEM images: (a) GO (b) 0.5:1 GO-T (c) 1:1 GO-T (d) 2:1 GO-T	46
Figure 4.5 EDS analysis: (a) Pure TiO ₂ (b) N- TiO ₂ (c) 0.1% Cu-NT (d) 0.5% Cu-NT (e) 1% Cu-NT (f) 2% Cu-NT (g) 3% Cu-NT	48
Figure 4.6 EDS analysis: (a) 0.5:1 GO-T (b) 1:1 GO-T (c) 2:1 GO-T	50
Figure 4.7 FT-IR spectra of (a) GO (b) 0.5:1 GO-T (c) 1:1 GO-T (d) 2:1 GO-T	52
Figure 4.8 Absorbance and Tauc plots of: (a) T (b) NT (c) 0.1%-NT (d) 0.5%-NT (e) 1%-NT (f) 2%-NT (g) 3%-NT	53
Figure 4.9 Tauc plots of: (a) 0.5:1 GO-T (b) 1:1 GO-T (c) 2:1 GO-T	54
Figure 4.10 Degradation spectra of methyl orange using all prepared photocatalysts	57
Figure 4.11 Plot between $\ln C_0/C_t$ vs time for MO	59
Figure 4.12 Activity of all prepared nanoparticles against methyl orange degradation	59
Figure 4.13 Efficiency of all prepared nanoparticles against degradation of MO	60
Figure 4.14 Degradation spectra of methyl orange using all prepared nanocomposites	61
Figure 4.15 Activity of all prepared nanocomposites again Methyl Orange degradation	62
Figure 4.16 Efficiency of all prepared nanocomposites against degradation of MO	63

List of Tables

Table 3.1 Details of TiO ₂ and doped-TiO ₂ photocatalysts	39
Table 3.2 Details of GO/TiO ₂ nanocomposites	39
Table 4.1 Average crystallite size of all prepared catalysts and composites	42
Table 4.2 Average particle size of all prepared samples	44
Table 4.3 EDS results: (a) Pure TiO ₂ (b) N- TiO ₂ (c) 0.1% Cu-NT (d) 0.5% Cu-NT (e) 1% Cu-NT (f) 2% Cu-NT (g) 3% Cu-NT	49
Table 4.4 EDS results of: (a) 0.5:1 GO-T (b) 1:1 GO-T (c) 2:1 GO-T	50
Table 4.5 Bandgaps of all prepared samples	55
Table 4.6 Degradation rate calculations for MO degradation using all catalysts under visible light irradiation	58
Table 4.7 Degradation rate calculations for MO degradation using all composites under visible light irradiation	64

List of Abbreviations

CB	Conduction Band
DRS	Diffuse Reflectance Spectroscopy
EDX	Energy Dispersive X-Ray Spectroscopy
eV	Electron Volt
FTIR	Fourier Transform Infrared Spectroscopy
GO	Graphene Oxide
hr	Hour
MO	Methyl Orange
mg	Milligram
ml	Milliliter
min	Minute
SEM	Scanning Electron Microscopy
UV-Vis	Ultra Violet-Visible Spectroscopy
VB	Valence Band
XRD	X-Ray Diffraction

1 INTRODUCTION

1.1 Background

For the past few centuries, scientists and researchers have been trying to develop environment friendly materials and using techniques to remove the hazardous and toxic pollutants and organic dyes from soil, air as well as water [1].

Dyes may be of classified in various categories based on their origin, usage and chemical nature. Dyes may have an acidic, basic or neutral nature depending on the type of application they are used for. They cause different types of pollutions and toxicity when they are exposed to environment [2].

Dyes also have several uses in industries for coloring different materials. But, the colored wastewater, when discharged into ponds, rivers and streams causes toxicity and hazardous problems to aquatic life as well as non- aquatic life [3]. This means that these industries are on one side providing human comfort but on the other side are endangering their lives. The degradation of these dyes is a necessary element for everyone [4].

Many methods and techniques have been used so far for the removal of these dyes from wastewater. All of these methods have certain pros and cons which make the researcher move towards new methods. Now, in the past few decades, researchers and scientists have been moving towards the idea of using natural energy sources to removes these hazardous materials in the easiest and cheapest possible ways [5].

For such strategies photochemical methods are proven to be better than the other. Photocatalysis and photodegradation are the most promising methods for the decomposition and degradation of these dyes [6]. These methods have more importance because they consume solar energy and are therefore considered environment friendly.

Many such methods have been introduced up till now for wastewater treatment, CO₂ reduction, H₂ production and purification of air [7].

1.2 Photocatalyst

Many semiconductors are used as a photocatalyst which include ZnO, CdS, WO₃, TiO₂ and many more. But, TiO₂ is proven to be the best photocatalyst so far due to its few

attractive properties and band gap of 3.2 eV [8]. Also, it is proven to have most amazing results for the degradation of dyes. This is because they are inexpensive, have thermal stability and non-toxicity [9]. On the other hand, they don't show any absorption in the visible region and only absorb the UV part of the sunlight which is present in lower percentage in sunlight. Another drawback of using TiO_2 is the fast recombination of electrons and holes takes place which causes the reaction to stop [10].

1.2.1 Mechanism of photocatalysis in TiO_2

What happens is that when such a semiconductor absorbs a photon of light having energy equal to or greater than the band gap of TiO_2 that is 3.2 eV, e^- from the VB of the semiconductor jumps to the CB and h^+ is left behind in the VB as shown in **figure 1.1**. The hole in the valence band has the oxidation potential of 2.6 eV which oxidizes water. The mechanism of this process is given below in equations {1} to {5} [11]:

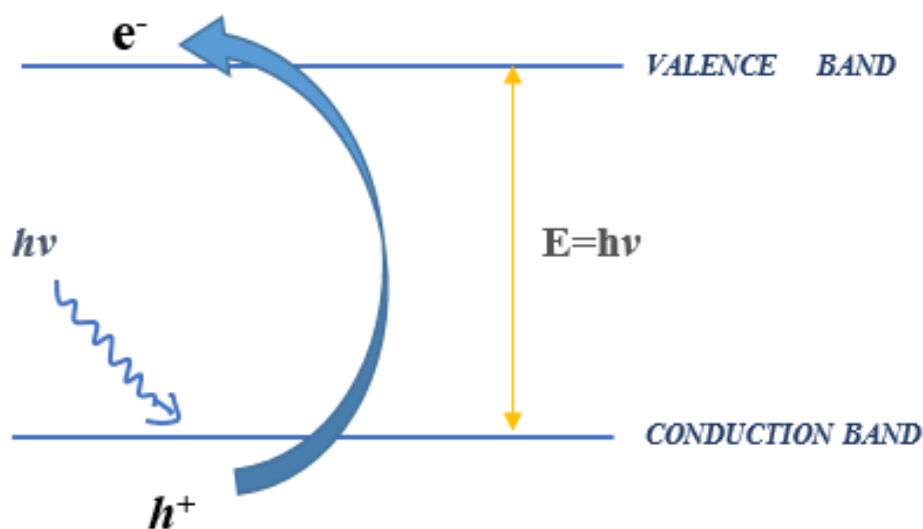


Figure 1.1 Illustration of basic mechanism of a photocatalyst



Now, if fast recombination is taking place or TiO_2 is absorbing the UV and near-IR part of the sunlight and not the visible part, then that calls for a problem which should be solved. So, the scientist and researchers have been working on improvement of TiO_2 since the discovery of TiO_2 as a best semiconductor but with few flaws. They have come up with all the best possible solutions, which include doping with metals, non-metals, and other semiconductors etc. [12]. Doping with certain elements reduces the band-gap of TiO_2 and hinders the fast recombination of electrons and holes as shown in **figure 1.2** [13].

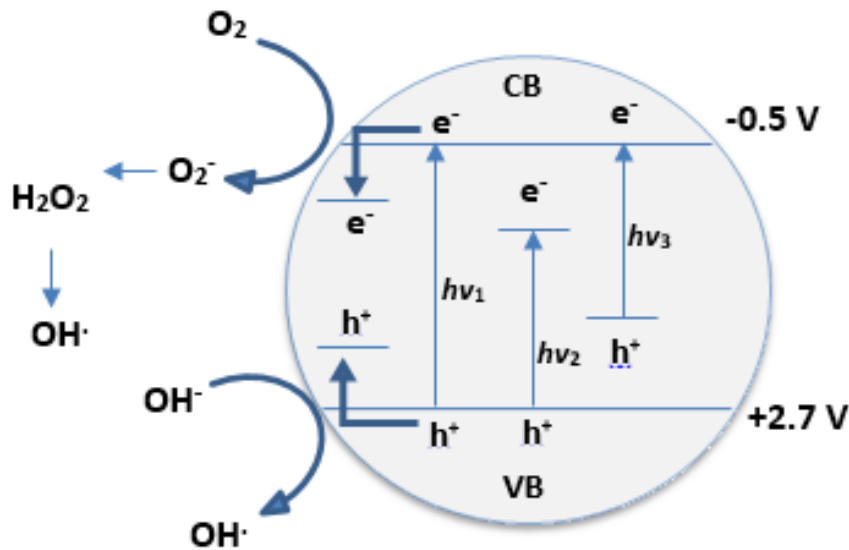


Figure 1.2 Mechanism of photocatalytic phenomena of TiO_2 . ($h\nu_1$: pure TiO_2 , $h\nu_2$: metal-doped TiO_2 , $h\nu_3$: nonmetal-doped TiO_2)

1.3 Doping

One of the best ways of reducing the band-gap of TiO_2 and almost hindering the fast recombination of electrons and holes is by doping with certain elements (metals, non-

metals and other semi-conductors). These kind of doping causes the band-gap to reduce to a level where visible light can be absorbed and eventually generation of e^-/h^+ pair occurs. [14]

1.3.1 Doping with metals

Metal dopants mostly include Pt, Fe, Ru, Co, Zn, V, Al, Ag and Cu etc., as these metals can modify the surface electronic properties. These metals can act as trapper of e^- and h^+ and also increase the photodegradation rate [15]. Among which most effective and widely used metal is copper (Cu) as it is inexpensive than remaining noble metals, its less toxicity, its relative abundance and high conductivity of electrons [16].

Many Cu-TiO₂ photocatalysts have been reported and used in photoremediation and photodegradation of certain toxic chemical, dyes and pesticides. Presence of copper as a dopant reduces the band-gap of TiO₂ and increases its activity. Cu metal can also be used for the treatment of wastewater [17].

1.3.2 Doping with non-metals

For the past 10 years TiO₂ has been doped with certain non-metals to improve its photocatalytic and photoelectrochemical properties. Non-metal doping elements are nitrogen, sulfur, carbon, fluorine, bromine and I [18]. When a non-metal doping is done, there are three things that occur:

1. Band gap of TiO₂ is narrowed to visible absorption range [19].
2. An impurity energy level is created which makes possible the absorption of visible light [20].
3. Oxygen vacancies are an important part of visible light activity. Any non-metal incorporation blocks the reoxidation [21].

Among all the non-metal dopant, N is considered to be the most promising and effective doping element for TiO₂. As, its atomic size is comparable with O, its ionization potential is very low, it is much stable and N doping in TiO₂ is more easy than other non-metals [22].

1.4 Graphene and graphene oxide

Carbon exists in many allotropic forms which can be described by their different shapes and dimensions [23]. These forms are given below and are also shown in **figure 1.3**:

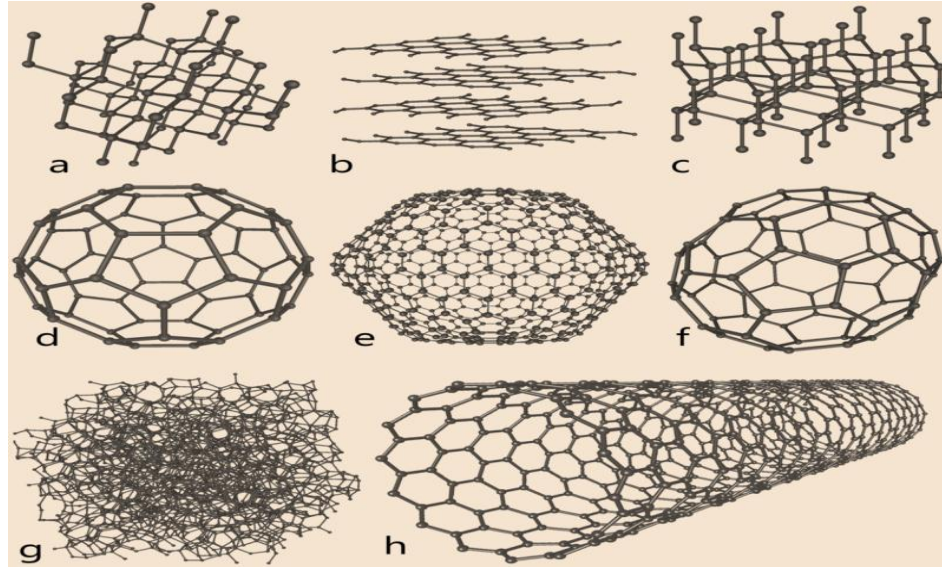


Figure 1.3 Allotropic forms of carbon: (a) Diamond, (b) Graphite, (c) Lonsdaleite, (d) Fullerene, (e) Fullerite, (f) Amorphous Carbon (g) CNTs

- a) Diamond
- b) Graphite
- c) Lonsdaleite
- d) Fullerene
- e) Fullerite
- f) Amorphous Carbon
- g) CNTs

Among all the mentioned allotropes of carbon, graphite in its exfoliated form is proven to be the most efficient than rest of the allotropes because of its exclusive electrical, thermal, mechanical and optical properties [24].

Graphene is a 2 dimensional exfoliated form of graphite which has a honey-comb like structure and has sp^2 -hybridized carbon atoms packed in a single sheet.

Graphene was isolated for the first time in 2004 by Kostya Novoselov and Andre Geim by using top down approach [25].

GO is an oxidized form of graphene. It is synthesized using oxidation and then exfoliation of graphite. The oxidation of graphitic layers results in the attachment of various functional groups on the carbon planes. These intercalated functional groups result in the weakening of the van der waal forces present between carbon planes. The oxidation of graphene is done in order to separate the layers of graphene by introducing oxygen groups [26].

In **figure 1.4**, it can be seen that graphite can either first be introduced with oxygen groups by oxidation and then the layers can be exfoliated, or they can be exfoliated first and then introduction of oxygen groups can be done.

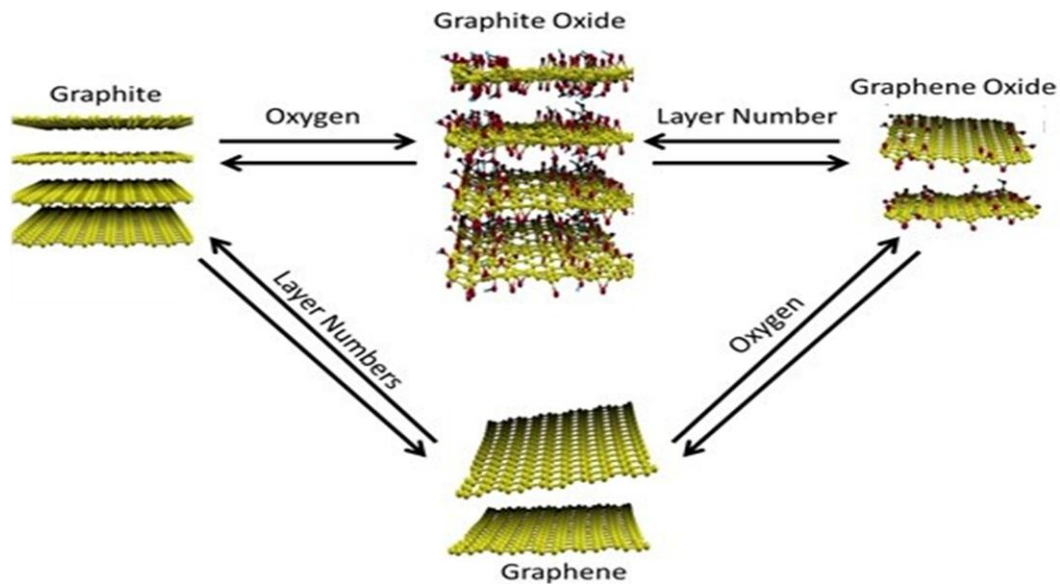


Figure 1.4 Exfoliation and oxidation of graphite into single layered graphene oxide

1.5 Graphene oxide and TiO₂ nanocomposites

The combination of GO and TiO₂ was done in order to obtain a composite that has properties of both a single layered material that has a larger surface area and a metal oxide that provide the facility of electron-hole generation easily [27]. Graphene based semiconductor photocatalysts were prepared for obtaining high specific surface area, great

electron conductivity and good adsorption and as a result improving the photocatalytic activity [28].

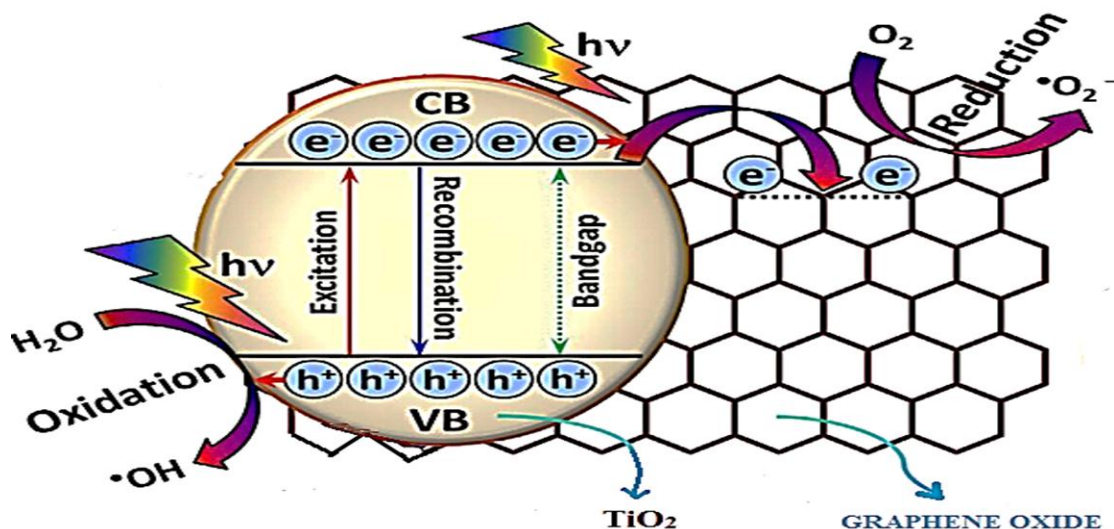


Figure 1.5 Scheme of GO-TiO₂ photocatalytic activity under UV-visible light

There are two types of carbon atoms in graphene oxide: Carbon atoms bonded to different functional groups and the carbon atoms involved in the formation of aromatic rings. The ratio of these two types of carbon atoms or regions illustrates how much oxidation is done. The functional groups are actually present on both sides of the plane. Hydrophilic nature of graphene oxide is because of these functional groups so stable aqueous dispersions can be made. Water molecules form hydrogen bonding with the covalently bonded oxygen molecules of graphene.

Figure 1.5 illustrates the excitation of electrons from VB to CB of TiO₂ by absorption of light. These excited electrons either recombine with the holes of VB or they are transferred to the CB of graphene sheet. The photocatalytic activity is increased due to decreased recombination of electrons and holes [29].

1.6 Synthesis routes for nanocomposite preparation

1.6.1 Synthesis routes for TiO₂

There are various methods by which TiO₂ has been synthesized depending upon the need of different morphologies and properties. Some methods proved to be best for the

synthesis of nanoparticles while others were found to be more efficient for the synthesis of other morphologies like nanorods, nanosheets, nanowires, nanotubes etc. [30]. Following are some of the methods that have been reported till date:

- a) Sol-gel method
- b) Hydrothermal and Solvothermal method
- c) Chemical vapor deposition
- d) Microwave method
- e) Sonochemical method

1.6.1.1 Sol-gel method

Sol-gel technique is a mature technique based on colloidal chemistry to obtain extraordinary and desired properties and it is a simple and cheap method. Sol is basically a colloidal suspension that contains solid particulates having range in few nanometers and the suspension is a liquid phase. Gel is formed when complete polymerization of the suspension takes place. This wet gel thus formed is then treated under heat and solid form is obtained. Ultrafine powder is obtained under calcination process. This process is widely used for the synthesis of metal oxide nanoparticles only if proper procedure and critical conditions are followed [31]. The scheme of TiO_2 nanoparticle synthesis through this method is shown in **figure 1.6**.

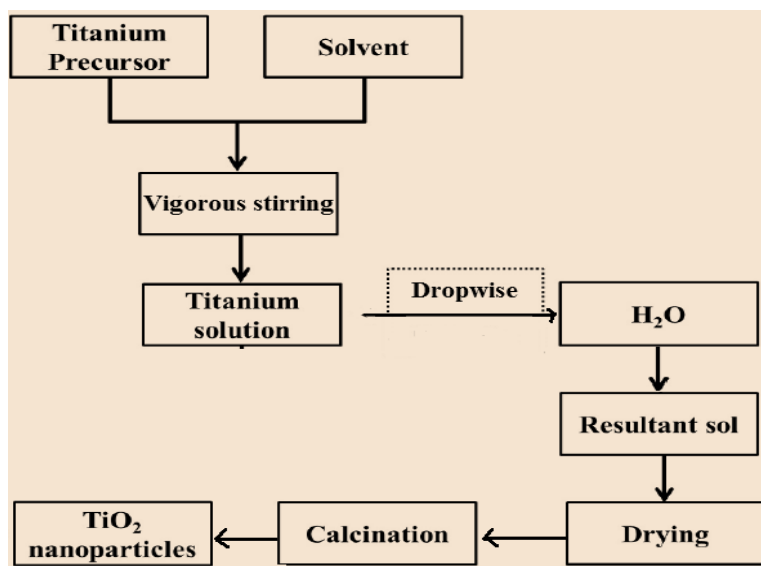


Figure 1.6 Scheme of TiO_2 nanoparticle synthesis via sol-gel method

1.6.1.2 Hydrothermal and solvothermal method

Hydrothermal process is performed mainly in autoclaves which are made of still and can have Teflon lining. This process is performed under highly optimum conditions that are control in temperature and pressure. This scheme is extensively used for the preparation of smaller particles in ceramic industry. Alongside nanoparticles, this process is best reported for the synthesis of nanotubes, nanorods and nanowires as well. In this process autoclave is filled with a precursor for metal oxide and a suitable solution and is sealed. This sealed container is then kept at suitable high temperature and pressure in an oven. The obtained sample is then filtered, washed and annealed at suitable temperature to obtain the nanostructures in highly fine powder form [32].

The only difference between solvothermal and hydrothermal method is the solvent that is used. It can also have a variety of temperature ranges and is mainly used only for the synthesis of nanoparticles [33].

1.6.1.3 Chemical vapor deposition

In this process, vapor-phase solutions are condensed to obtain a solid-phase material. This process is extremely used when coatings are to be formed in order to change the electrical, thermal, optical and mechanical properties of different substrates. Thermal energy is used in this process to heat the gas in chamber and start the deposition process. Under defined parameters, nanostructures of the given material can be obtained [34].

1.6.1.4 Microwave method

In this process as the name suggests, electromagnetic waves of high frequency and low energy are used. The range of frequencies is from 900 MHz TO 2450 MHz under which microwave heating takes place. These microwave radiations are applied in order to prepare nanostructured materials. This method is very simple and neat and there is no problem in the effect of thermal gradient [35].

1.6.1.5 Sonochemical method

In this process ultrasonic bath is used for the synthesis of nanostructured materials. In a typical defined process, a solution of metal oxide precursor and a suitable solvent is stirred for two hours keeping the temperature normal. The obtained solution is then treated under ultrasonic bath irradiation for defined time and temperature. The obtained solution was

then centrifuged and decanted and at the end tried at given temperature to obtain desired nanostructured materials [36].

Among all the above mentioned processes and many other processes for the nanoparticle synthesis, sol-gel method is proven to be the best, easier and cheapest method for the synthesis of doped or un-doped TiO₂ nanoparticles.

1.6.2 Synthesis routes for graphene and graphene oxide

There are various methods used for the preparation of graphene. Exfoliation method among these methods is proven to be best for the synthesis of graphene sheets. The first method was discovered by using adhesive tape and separating single layer of graphene. As time passed, new and modified methods were discovered. **Figure 1.7** shows the different synthesis routes of graphene.

Mechanical and chemical exfoliation methods mostly due to their ease of availability and their inexpensive and easier processes [37].

The method used for the synthesis of graphene oxide is chemical method among which the most widely used method is hummers' method.

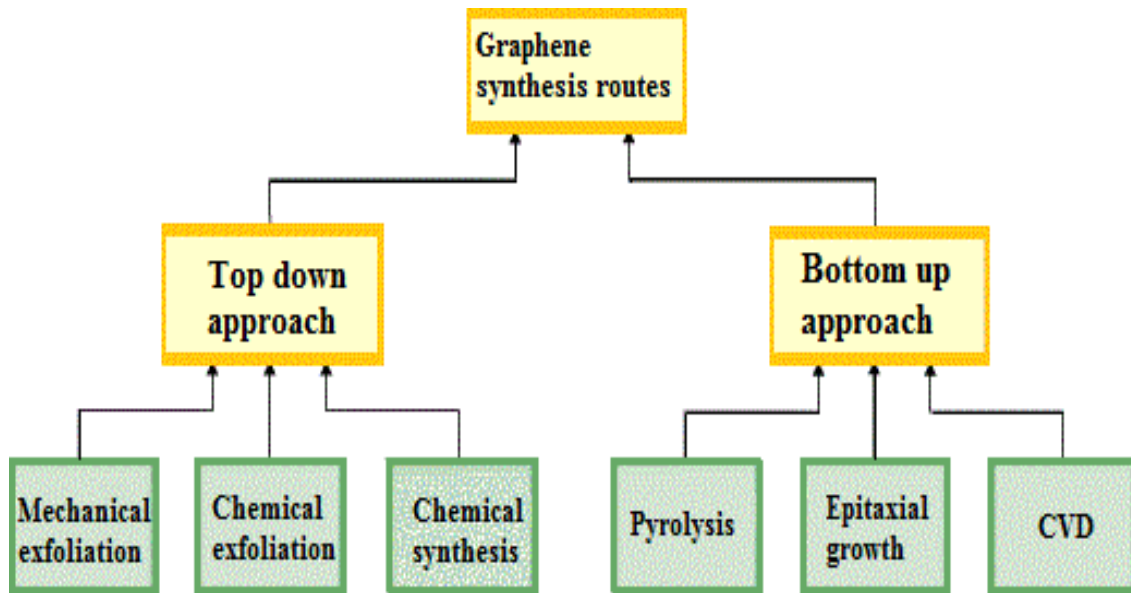


Figure 1.7 Flow sheet diagram for different synthesis routes of graphene

1.6.2.1 Hummers' method

This process is extensively used basically for the synthesis of graphene in its oxidized form. This method is best suitable for the creation of more defects in graphene surface. It is an easy and inexpensive method.

Steps involved in this method [38]:

1. Addition of NaNO_3 and H_2SO_4 to graphite powder under continuous stirring for 2 hours and at low temperature up to 5°C .
2. After 2 hours stirring, addition of KMnO_4 is done slowly and after that temperature is maintained to 35°C and the solution is kept under stirring for 2 days.
3. After 2 days stirring grey slurry is formed, after which addition of water is done slowly and which is then moved to addition of H_2O_2 and the reaction is terminated.
4. The obtained solution is settled down and decanted, sonicated, washing with HCl and H_2O was done several times and then drying was done oven for 24 hours to obtain graphene oxide.

1.6.3 Synthesis routes of graphene-metal oxide nanocomposite

1.6.3.1 Microwave heating

Microwave heating is quite different from ordinary heating so use of this technique for the synthesis of nanostructures is more dependent on the properties of material being used rather than process conditions. For a very short time highly localized heating results in the formation of very fine particles [39].

1.6.3.2 In-Situ chemical synthesis

This method is very much suitable for the preparation of graphene/inorganic nanostructure composite. The very first step for the synthesis of nanocomposite by this technique is the interaction between positively charged metal atoms and negatively charged electron cloud of oxygen atoms bonded with GO [40].

1.6.3.3 Hydrothermal and solvothermal method

It is a famous method for the synthesis of nanostructures at high temperature and pressure. The process is carried out in a closed system and mostly the solvent used is water so this technique is considered as environmental friendly. Highly pure crystals can be formed in

bulk amount depending on the capacity of the vessel of autoclaves so this method gains a lot of interest by the researchers. There are many reports for the synthesis of graphene/inorganic nanostructures composites based on this technique: CuO/graphene [41], ZnO/graphene [42] and SnO₂/graphene [43].

It is not compulsory to use water as a solvent some other solvents can also be used like ethanol, methanol etc. This technique is known as solvothermal technique, when water is used as a solvent.

1.7 Dyes

Dyes are sort of pigments which are used to color different substances but mostly used on fibers and leather made products. Dyes are aromatic organic compounds and have affinity for the particular substances. Most of the dyes are used in the form of aqueous solutions. The solubility of dyes in water is because of the auxochromes i.e. -OH, -Cl, -Br, -NO₂, -COOH, -NHR, -NH₂ etc. Auxochromes have the ability to ionize in water thus making dyes soluble and these groups are also responsible to intensify colors of dyes. Auxochromes can be classified based on their charge and nature i.e. acidic or basic [44].

1.7.1 Color of dyes

Dyes are organic aromatic compounds but they pose colors [45] because:

- They absorb light in visible region.
- They have color bearing groups (chromophores).
- They exhibit resonance of electrons.
- They have a conjugated system.

1.7.2 Types of dyes

Mainly dyes are classified as:

- a) Natural dyes
- b) Synthetic dyes

Animals and plants are the sources of natural dyes. Like Tyrian purple and madder are natural dyes extracted from sea snails and madder root respectively. Synthetic dyes are classified as non-azo dyes and azo dyes. Azo dyes are further classified as acidic, basic,

and reactive, disperse and Sulfur dyes. Synthetic dyes can also be classified as basic and acidic based on their nature. **Figure 1.8** shows the flow chart for the classification of dyes.

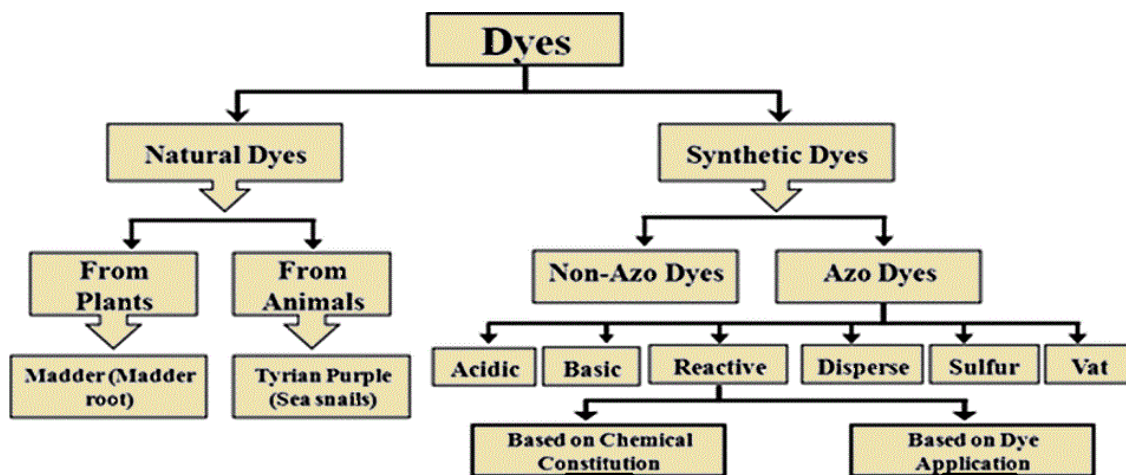


Figure 1.8 Flow chart for classification of dyes

1.7.3 Need for dye degradation

Although dyes have many benefits but they are also dangerous to human life in many different ways. Following are the several hazards of dyes [46]:

- Dyes are most of the times soluble in water and thus they cause pollution in water. This water when discharged in to rivers, it causes severe damage to aquatic as well as human life.
- Dyes affect the absorption and reflection of sunlight from water thus affects the underwater photosynthetic activity.
- A lot of dyes are carcinogenic and some can cause irritation to skin.
- Transparency of water bodies are greatly affected by the small amount of dyes which are even undetectable by human eye.

So, these harmful dyes need to be removed or better, degraded for the survival of living beings.

1.7.4 Methyl orange

Methyl orange is an orange color dye and mostly used as pH indicator as it changes its color from orange to yellow when present in more basic solutions.

The molecular structure of methyl orange is changed when the pH of the solution is changed which is indicated by the change in color of methyl orange. In acidic conditions hydrogen ion is attached to the nitrogen atom of N=N bond thus changing the molecular structure [47]. There are basically two colored forms of methyl orange as shown in **figure 1.9**:

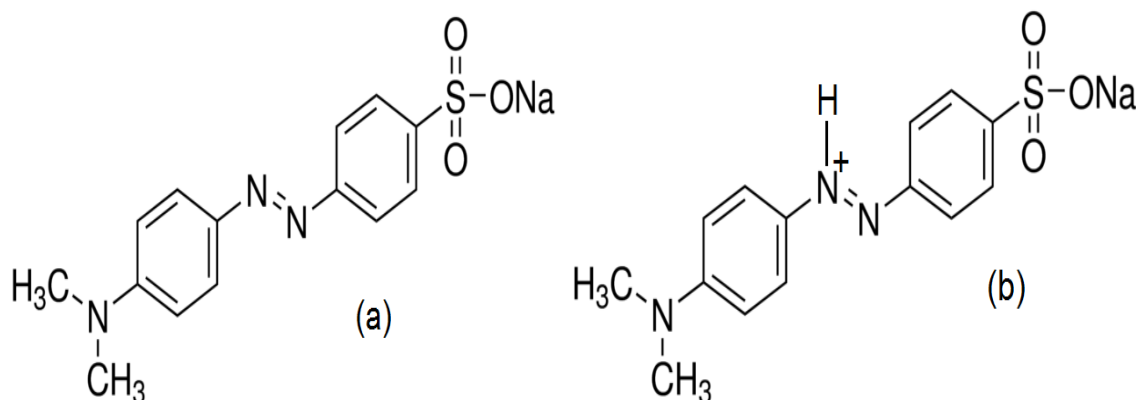


Figure 1.9 (a) Yellow form of methyl orange (b) Red form of methyl orange

1.7.5 Dye degradation mechanism by photocatalyst

In **figure 1.10**, it can be seen that the dye is being degraded in every possible way just after the photocatalyst is irradiated and electron-hole pair generation takes place. The electrons in the CB of the semiconductor degrade the dye.

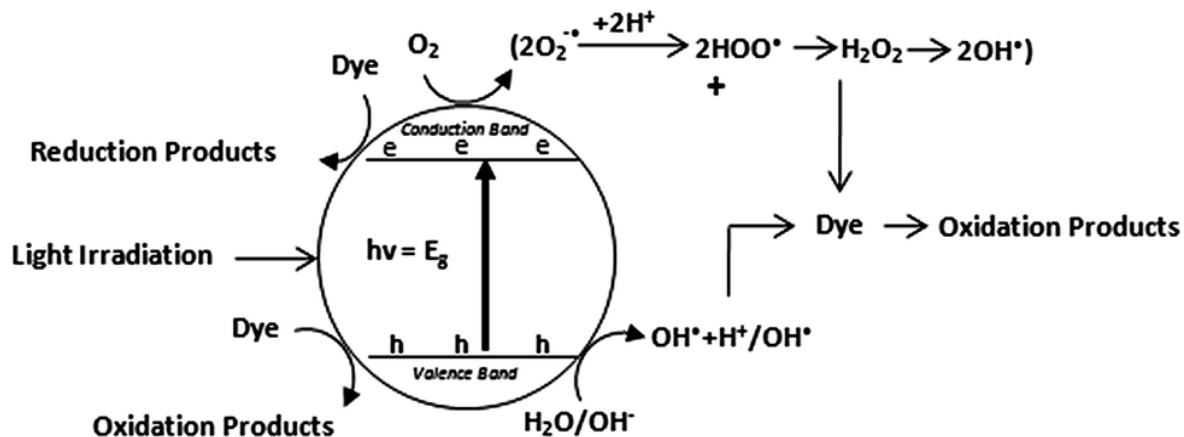
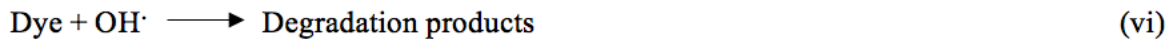


Figure 1.10 Schematic illustration of photodegradation of dye under light irradiation

The valence band (VB) holes play an integral role to induce oxidative decomposition of environmental pollutants via photocatalytic oxidation reaction. The holes present in valence band can directly oxidize pollutants but they react with water to form hydroxyl radical (OH^\cdot) [48].

The basic mechanism of pollutant degradation is shown in the following equations from (i) to (viii):



Large amount of photocatalysts have been developed since today for the removal of pollutants and organic dyes from water.

1.8 Characterization techniques

Once the nanomaterials are synthesized, the next step involves the analysis of phase purity, particle size, crystallite size, surface morphology, elemental composition and optical properties. This can be done by using various techniques comprising powder X-ray Diffractometry, Transmission and Scanning Electron Microscopy, Thermogravimetry, Infrared Spectroscopy, UV-Visible spectroscopy, Electron Spin Resonance spectroscopy. They will be discussed briefly in the following section.

1.8.1 Scanning electron microscopy (SEM)

Basic principle

SEM is one of the important characterization techniques as it is capable of producing high resolution images of the surface of the sample. These images are created in such a manner that they produce a 3-dimensional appearance which is very useful to judge the morphology of the sample.

Mechanism

Its basic functioning depends on the thermionically emitted electrons from a tungsten source and that move towards an anode as can be seen in **figure 1.11**. The whole system is maintained under a very high vacuum. The electron beam having an energy (-50 keV) is focused by one or two condenser lenses with a highly fine focal spot size (1 nm to 5 nm). The images generated by the SEM are of three types including: (i) Secondary electron images (ii) Backscattered electron images and (iii) Elemental X-ray maps. The electrons are referred as secondary electrons if their energy is less than 50 e V. The secondary electrons are emitted from the few nm of the surface and hence provide the information about the surface.

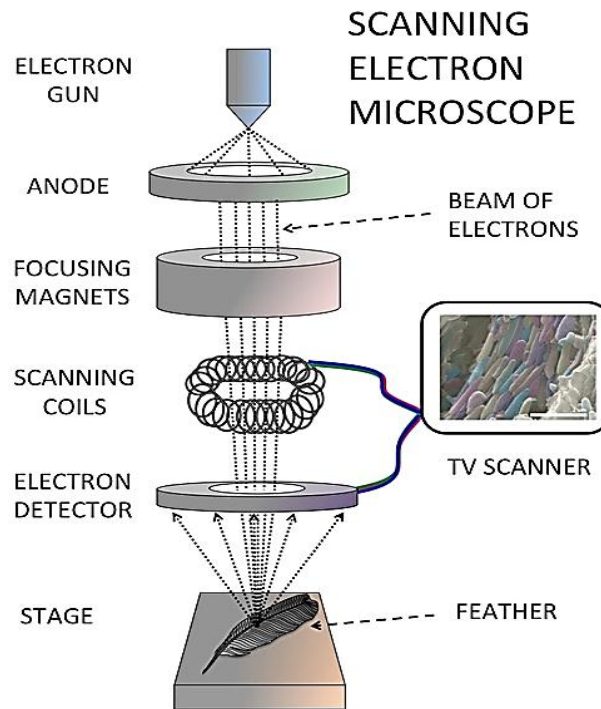


Figure 1.11 Schematic illustration of SEM

1.8.2 Energy dispersive X-ray spectroscopy (EDS or EDX)

Basic principle

Its characterization ability is based on the principle that each element has a unique atomic structure that allows X-rays that are characteristic of an element's atomic structure for identification.

Mechanism

When an incident beam is allowed to fall on a sample, it excites an electron from an inner shell, which creates a hole in the shell after ejection. As a result an electron from an outer shell falls into the inner shell to fill that vacancy. The energy difference between the higher shell and the lower shell results in emission of X-rays.

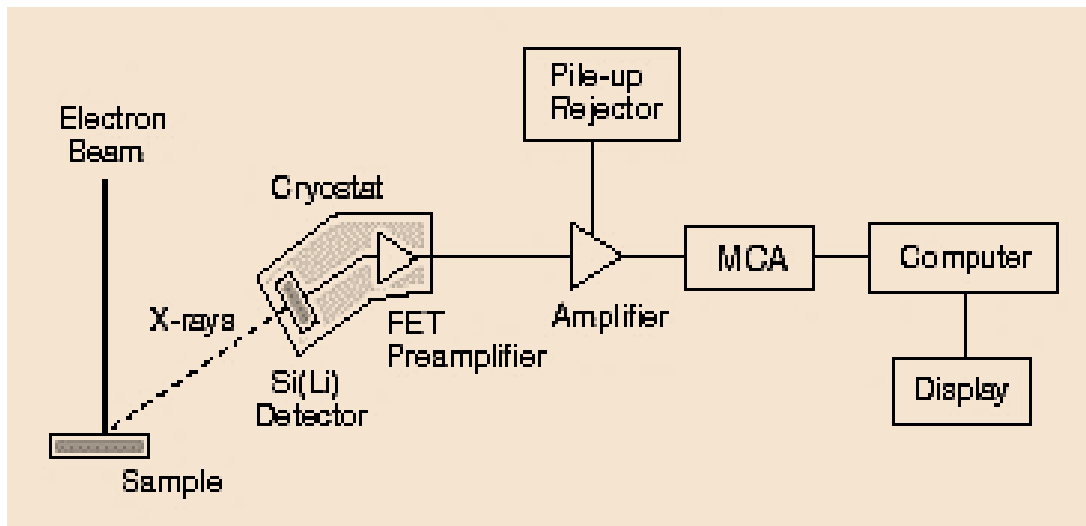


Figure 1.12 Schematic illustration of EDS/EDX

The number and energy of the X-ray emitted from a sample is measured by an energy dispersive spectrometer. As the energy of the X-rays is specific for an element, this allows the measurement of elemental composition of the specimen. **Figure 1.12** illustrates the basic scheme of EDX machine.

1.8.3 X-ray diffraction (XRD)

Basic principle

X-ray diffraction is considered as one of the most efficient technique used for identification of the crystalline phase of the materials. It can also be used to measure the phase composition, preferred orientation, grain size, strain state and structural defects of these phases.

Mechanism

In this technique a beam of X-rays of a specific wavelength (λ) is focused on the crystal at an angle θ to the atomic planes. These X-rays interact with the electrons of the atoms and are reflected back by the atomic planes. As the atomic planes of the crystal structure are considered to be semitransparent, they allow a part of the X-rays to pass through and reflect the other part. The incident angle θ is equal to the reflected angle as shown in **figure 1.13**; it is also called Bragg angle.

Bragg's law: $2d\sin\theta = n\lambda$

The particle size of crystallites can be determined by applying Scherrer's formula.

Scherer's formula: $D = K \lambda / B\cos\theta$

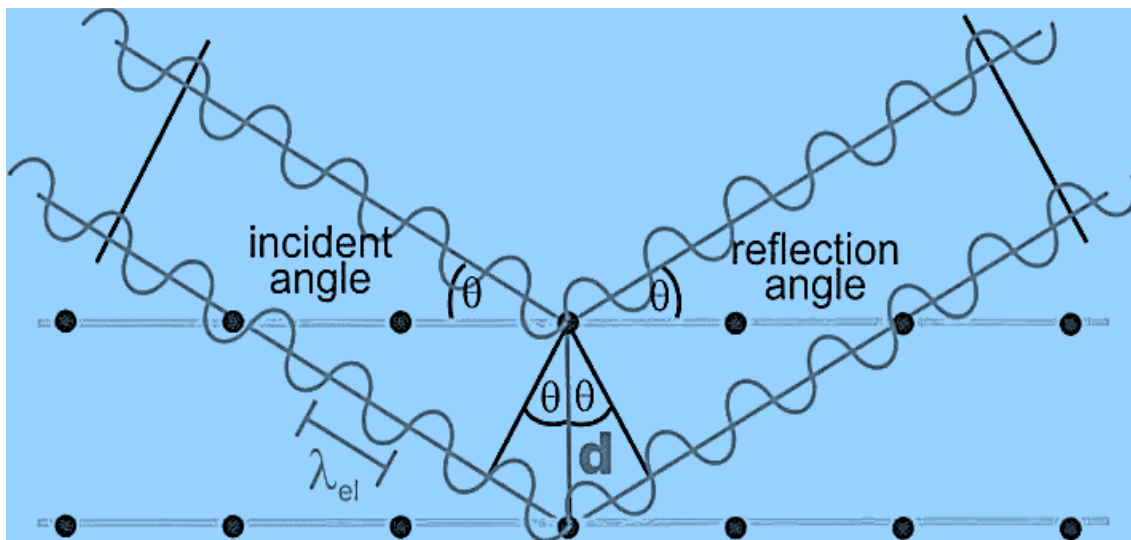


Figure 1.13 Bragg's law of diffraction

The characteristic X-rays that come from an X-ray generator are collimated and directed onto the sample. Afterward, the sample and detector are rotated to record the intensity of the reflected X-rays, which is further processed by a detector. The function of the detector is to convert the signal and then sent to a monitor of the computer. Inside the XRD machine, there is an instrument known as goniometer which is used to maintain the angle and rotate the sample. Cu and Ni filters are used to stop the unwanted radiation.

1.8.4 Fourier transform infrared spectroscopy (FTIR)

Basic principle

The basic principle of infrared spectroscopy is based on the vibrational motion of the molecules which originate due to the difference in dipole moment with in the same or different molecules. These vibrational frequencies act as fingerprint for characterizing organic, inorganic and biological compounds.

Mechanism

FTIR is considered as non-destructive technique that is used to get the information about the chemical bonding for solids and thin films.

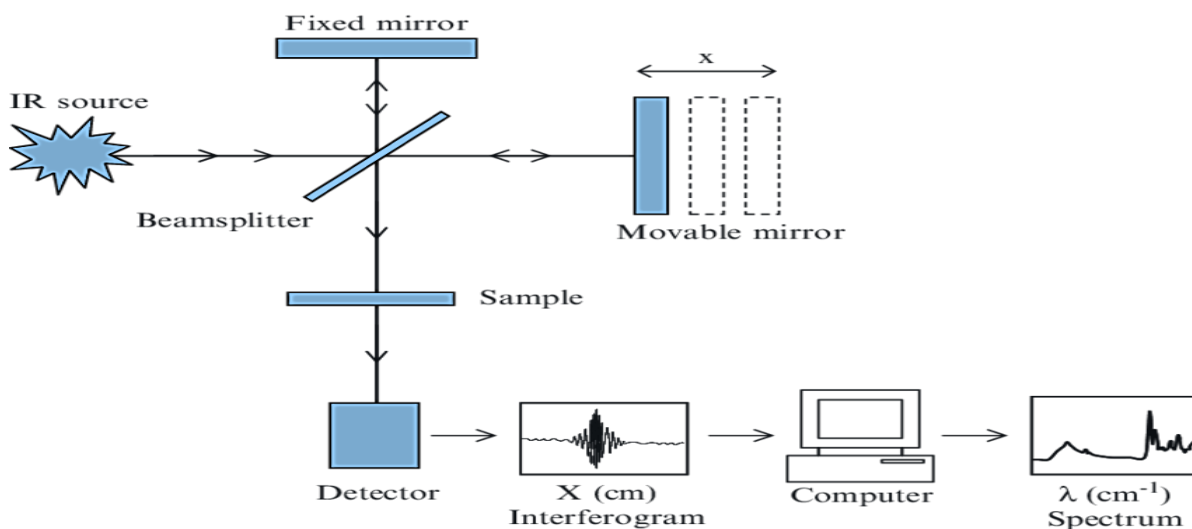


Figure 1.14 Schematic illustration of FTIR spectrometer

Basically, it measures the changes in the intensity of a beam of infrared radiation with respect to the wavelength or frequency after its interaction with the sample. It also

measures the ratio of intensity of sample before and after striking. The plot of this ratio versus frequency is called infrared spectrum.

As the band intensities are proportional to the concentration of the compound, so FTIR can also be used for the quantitative analysis of the sample. The range of FTIR spectrophotometer lies between $4000\text{-}450\text{ cm}^{-1}$. The sample used for the characterization is ground with KBr to form a pallet and the signal is sent to the detector and is recorded in computer as can be seen in **figure 1.14**.

1.8.5 UV-visible absorption spectroscopy

Basic principle

Absorption spectroscopy deals with the absorption of photon by the material when the frequency of light is in resonance with the energy difference between states as per allowed selection rules. The electronic structure in emission spectroscopy is determined through excitation of electrons from the ground to the excited states and then relaxation from the excited to the ground state.

Mechanism

A characteristic absorption spectrum of the sample is obtained by measuring the absorption of the sample with respect to the frequency of light. The characteristic lines observed in the absorption spectra of isolated atoms are very sharp which helps in the determination of the wavelength of photon accurately.

These lines are characteristic of a particular atom or ion for its identification. As there is age degeneracy in solids at atomic levels it gives broad optical spectra. The energy difference between the highest occupied molecular orbital (HOMO) and the lowest unoccupied molecular orbital (LUMO) bands is designated as the fundamental gap. As the penetration depth of UV/Vis spectroscopy is only of the order of 50 nm, so it cannot be used for the bulk solid, though, this technique is highly applicable for characterizing nanomaterials.

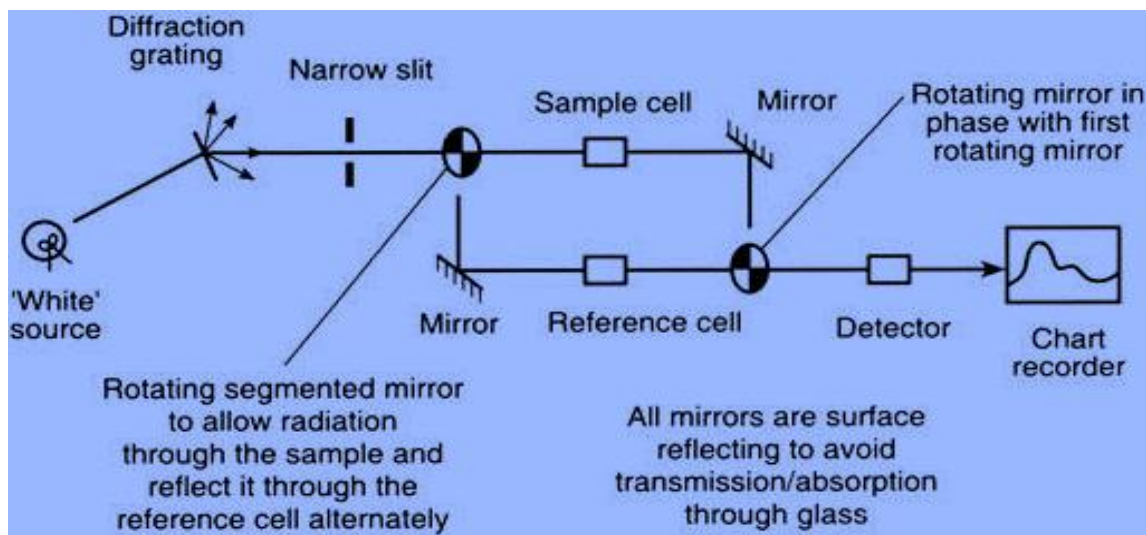


Figure 1.15 Schematic illustration of UV/visible spectrometer

The absorption spectra of UV/Vis spectrometer ranges from 200 nm to 800 nm. The spectrometer contains double beam along with double pass monochromator with good resolving power.

The light beam coming from Deuterium lamp passes through the filter and is focused onto a grating by a concave mirror. This beam is again reflected by grating. The reflected beam is then directed to a partial reflecting mirror which further splits the beam into two paths, one passes through the sample and the other through the reference material and finally focused on the detector. This scheme is illustrated in **figure 1.15**.

1.9 Objectives of this work

This thesis describes an effort to make TiO₂ nanoparticles by using sol-gel synthesis method. The objective was to make a photocatalyst and a nanocomposite that is visible light active and can be easily used for the degradation of dyes.

Following are detailed objectives of this thesis:

1. Synthesis of TiO₂ nanoparticles by sol-gel method.
2. Synthesis of N-doped and N/Cu co-doped TiO₂ nanoparticles by sol-gel method.
3. Characterization of all the prepared samples.
4. Choosing the best catalyst by performing degradation studies of Methyl Orange.
5. Synthesis of Graphene oxide nanosheets by Hummers' method.
6. Synthesis of nanocomposite of Graphene Oxide and best catalyst by hydrothermal method.
7. Performing some degradation studies and comparing their studies.

2 LITERATURE REVIEW

This chapter involves all the literature that was reviewed before and during this thesis work. There are a lot of research been done on nanoparticle synthesis and their doping, nanocomposite synthesis and degradation of different type of dyes. This thesis includes all the literature already done on TiO₂ synthesis, its doping, its composite formation and degradation of methyl orange involving these photocatalysts.

2.1 TiO₂ nanoparticles

In 1972, Fujishima and Honda discovered the water splitting phenomena by using semiconductor TiO₂ [49]. Since that discovery TiO₂ has been extensively used in different morphologies for photocatalytic activity. TiO₂ nanoparticles out of all the other morphologies have proven to be the best in performing photocatalytic activities [50]. In 1977, Frank and Bard used that water splitting technology for the reduction of cyanide ion [51]. TiO₂ increases the surface area, so this work includes the use of TiO₂ nanoparticles. For the synthesis of TiO₂ nanoparticles many methods are used up till now. But sol-gel among all these methods was confirmed to be best for the synthesis of nanoparticles.

- **Sol-gel method**

Chen-Chi Wang and Jackie Y. Ying (1999), reported the synthesis of TiO₂ nanoparticles for the first time via sol-gel method. They examined all the optimum conditions and parameters that were needed to be controlled for the formation of highly fine, nano-sized and non-agglomerated particles. The heat treatment was also studied, as that affected the crystallinity of the particles. Nanoparticles up to 6 nm small size in anatase form were obtained via this method by controlling all the parameters [52].

Huaming Yang, Ke Zhang and Rongrong Shi (2006), reported the sol-gel synthesis route for TiO₂ nanocrystal preparation and their photocatalytic study for the degradation of methyl orange. The crystal size that was calculated from XRD analysis was almost 16 nm and the calcination temperature was kept at 500 °C. The increase in temperature from 500 °C showed both anatase and rutile phase characteristics. Methyl orange degradation studies showed better results for anatase phase than the rutile phase. Also the control in pH,

hydrogen peroxide addition and TiO₂ reusability affected the rate of photodegradation of methyl orange [53]. The schematic illustration of whole process can be seen in **figure 2.1**.

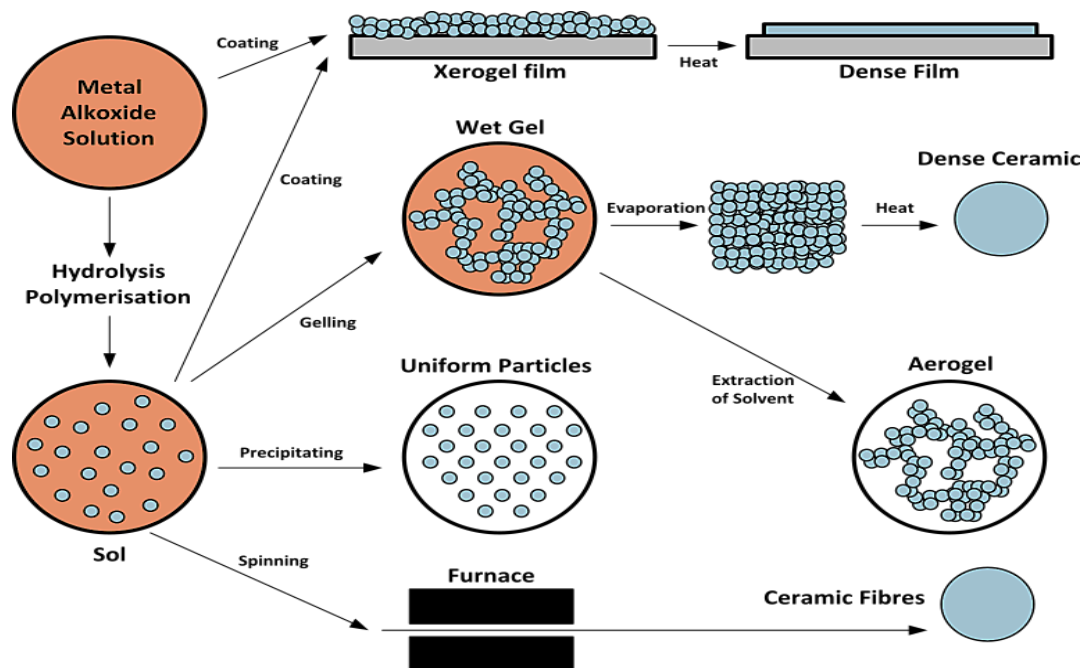


Figure 2.1 Schematic illustration of steps involved in sol-gel method

M. Hamadani, A. Reisi-Vanani and A. Majedi (2010), reported TiO₂ and Cobalt doped TiO₂ nanoparticles synthesized by sol-gel route including ultra-sonication treatment. Anatase phase was only obtained for all the samples that were prepared. All the characterization techniques that were performed, confirmed the TiO₂ nanoparticles and the ones doped with cobalt. The doped TiO₂ showed lower activity for doped TiO₂ than undoped TiO₂ [54].

R. Vijayalakshmi and V. Rajendran (2012), reported the synthesis of TiO₂ nanoparticles via sol-gel method and hydrothermal method. They concluded all the results and confirmed that TiO₂ nanoparticles produced through sol-gel method were more crystalline and they had crystallite size nearly equal to 7 nm. Whereas, TiO₂ nanoparticles produced by hydrothermal treatment were having crystallite size almost 17 nm which was much higher than the previous method. Bandgap for both sized nanoparticles depended on the crystallite size [55].

Ajay Sharma, R.K. Karn and S.K. Pandiyan (2014), reported the synthesis of nanostructured TiO₂ through sol-gel method by simple hydrolysis of Titanium Isopropoxide. The prepared nanoparticles were having crystallite size of approximately 20 nm. The nanoparticles had both anatase and rutile phase mixture which was confirmed by using XRD technique. SEM was used to study the morphology and particle size of the samples prepared. The spherical morphology was only observed in the case of anatase phase. The calculated band gap for this phase was about 3.2 eV [56].

Raad S. Sabry, Yousif K. Al-Haidarie and Muhsin A. Kudhier (2016), reported the successful synthesis of anatase phased TiO₂ nanoparticles using TiCl₄ as precursor. This method is inexpensive and is an easy approach with performance done at room temperature. When TiO₂ was calcined at higher temperature and the gel formation time was increased, the crystallite size was also increased and it was confirmed through XRD data. Degussa-P25 showed decreased efficiency, whereas, TiO₂ nanoparticles synthesized via sol-gel showed increased efficiency for the degradation of methylene blue. This improved efficiency was due to the large specific surface area of prepared nanoparticles [57].

2.2 Nitrogen doped TiO₂

M. Sathish, B. Viswanathan and R. P. Viswanath (2004), reported the synthesis of nitrogen doped TiO₂ nanoparticles using simple chemical route and calcination temperature of 400 °C. The nanoparticles that were obtained had homogenous size of 14 nm approximately and were spherical in shape. This method was more efficient than other methods for two specific reasons: (i) Low cost method and precursors were used for the synthesis of nitrogen doped TiO₂ nanoparticles. (ii) The TiO₂ nanoparticles formed were uniform in size and shape. N-doped TiO₂ nanoparticles showed better photocatalytic activity for the degradation of methylene blue than Degussa-P25 and pure TiO₂ nanoparticles under visible light [58].

Yu Huan, Zheng Xuxu and Yin Zhongyi (2007), reported the successful synthesis of nitrogen doped TiO₂ nanoparticles using sol-gel treatment. Ammonium chloride was used as a source for nitrogen and the calcination was done at specific temperature. The studies showed the effect of pH and specific calcination temperatures on particle size of the

nanoparticles which also affected the overall photocatalytic activity. Schematic representation of UV and Visible light absorption of N-doped TiO₂ can be seen in **figure 2.2**. The perfect results for photocatalytic activity were obtained when calcination temperature was kept 500 °C and the pH was kept 3. The nitrogen doped TiO₂ nanoparticles showed improved activity than the undoped TiO₂ nanoparticles for the degradation of 4-chlorophenol under visible light [59].

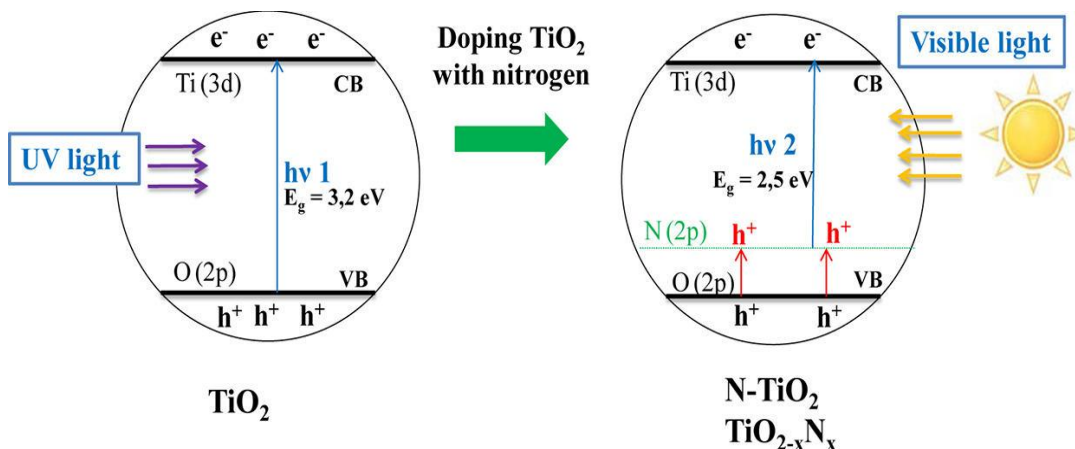


Figure 2.2 Schematic representation of UV and visible light absorption of N-doped TiO₂

J. Senthilnathan and Ligy Philip (2010), reported the photocatalytic activity using nitrogen doped TiO₂ nanoparticles under irradiated visible light. Modified sol-gel method was used for preparation of these doped TiO₂ nanoparticle photocatalysts. Triethylamine was used as a nitrogen precursor for doping in TiO₂ nanoparticles. Different characterization confirmed the doping of nitrogen and the calculations from XRD results gave the crystalline size of about 22 nm. In this study, XPS data showed the replacement of oxygen atom in TiO₂ lattice by nitrogen atom. Lindane was degraded using the prepared photocatalyst using visible light irradiation. N-doped TiO₂ nanoparticles proved to give best results for degradation. Lindane was completely degraded and it was confirmed through GC-MS analysis [60].

Armineh Hassanvand, Morteza Sohrabi and Sayed Javid Royae (2014), reported the synthesis of nitrogen doped TiO₂ nanoparticles by simple and direct impregnation method by applying amination over bulk TiO₂ (Degussa-P25). These prepared doped TiO₂

nanoparticles were then characterized using different techniques. These techniques confirmed the presence of both anatase and rutile phases in the prepared nanoparticles. SEM image of C/N co-doped TiO₂ nanoparticles are shown in **figure 2.3**. Comparison of both, the prepared catalyst and bulk TiO₂ was studied by the degradation of phenol under visible light irradiation. Nitrogen doped TiO₂ nanoparticles showed improved photocatalytic activity as compared to bulk TiO₂ [61].

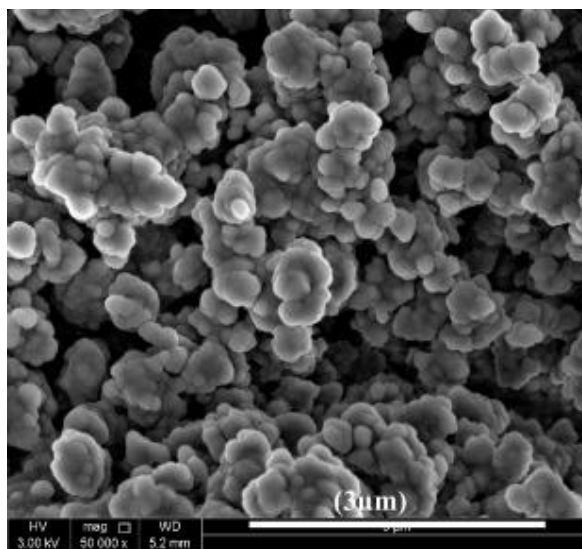


Figure 2.3 SEM image of C/N co-doped TiO₂ nanoparticles

Aboubakr M. Abdullah, Noora J. Al-Thani and Khoulood Tawbi (2016), reported the synthesis of carbon and nitrogen co-doped on TiO₂ and carbon tetrachloride and polyaniline were used respectively as precursors. The calculated particle size from SEM images was 35 nm to 40 nm. Different characterization techniques were done to confirm the incorporation and nitrogen and carbon. The prepared photocatalyst showed increased efficiency for the degradation of phenol than bulk TiO₂ and pure TiO₂ under UV light irradiation [62].

2.3 Copper and nitrogen doped TiO₂

Kaixi Song, Jiahong Zhou and Jianchun Bao (2008), reported the sol-gel synthesis of copper and nitrogen co-doped TiO₂ nanoparticles. Different characterization techniques were performed and incorporation and copper and nitrogen both were confirmed. The

absorption range for doped catalyst was shifted from UV to visible region nearly equal to 590 nanometers. The photocatalytic activity for doped TiO₂ nanoparticles was increased for degradation of xylenol orange than for bare TiO₂ nanoparticles or for individually doped nitrogen and copper on TiO₂ nanoparticles [63].

Rosendo Lopez, Ricardo Go´mez and Maria Elena Llanos (2010), reported the synthesis of copper doped TiO₂ nanoparticles by sol-gel method. Nanocrystalline anatase form of crystals was formed that had crystalline size of nearly equal to 30 nanometers. In the XRD graphs, a shift in 2θ was clearly observed, which confirmed the incorporation of copper in TiO₂ lattice. Bandgap shift was also observed in the case of doped TiO₂ nanoparticles than in pure TiO₂ nanoparticles from 3.19 eV to 2.81 eV. Different concentrations for copper were used for doping and high photocatalytic activity was observed in case of highest concentration of copper doped TiO₂ nanoparticles [64].

R. Jaiswal, J. Bharambe and N. Patel (2014), reported the synthesis of nitrogen and copper co-doped TiO₂ nanoparticles to improve the photocatalytic absorption of TiO₂ nanoparticles. The TiO₂ nanoparticles were able to absorb visible light and electron-hole recombination was lowered by doping with both a metal and a non-metal. Different percentages were used for nitrogen and copper doping separately and the best concentrations selected were then co-doped on TiO₂ nanoparticles to obtain the perfect results of degradation of methylene blue. Simple nitrogen doping reduced the bandgap up to 3.0 eV whereas, doping with copper reduced the bandgap up to 2.2 eV [65].

Paruchai Pongwan and Khatcharin Wetchakun (2016), reported the successful synthesis of different concentrations of copper doped TiO₂ nanoparticles via sol-gel method from 0.5 mol% to 5.0 mol% and compared them with bare TiO₂ nanoparticles. The best results were obtained when 2.0 mol% of copper doped TiO₂ nanoparticles were studied. The 2 mol% of copper on TiO₂ nanoparticles shifted the bandgap to 2.88eV as can be seen in **figure 2.4**. Also, the best photocatalytic studies for mineralization of oxalic acid and formic acid was also best achieved by the same concentration of copper. The reason behind this improved activity was given to the electron trapping by copper and reduced e⁻/h⁺ recombination [66].

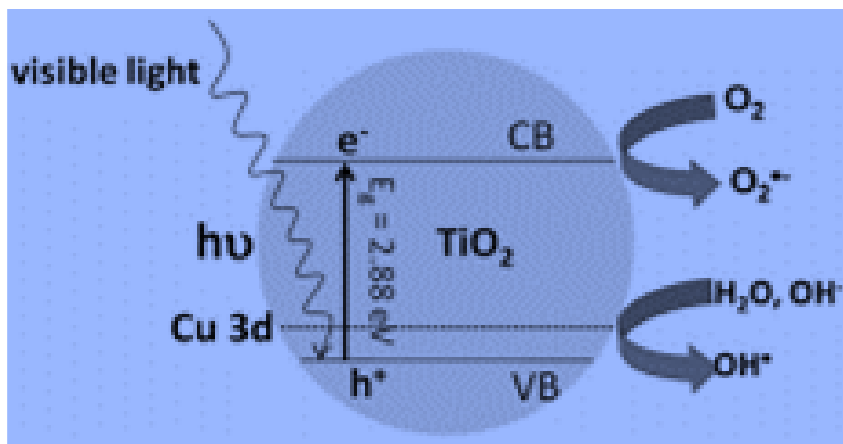


Figure 2.4 Schematic illustration of copper doped TiO₂ based photocatalysis

S. M. Reda, M. A. Khairy and M. A. Mousa (2017), reported the synthesis of nitrogen, copper and nitrogen/copper co-doped TiO₂ nanoparticles through microwave assisted sol-gel method. The particles produced by this method were all having spherical morphology and particle size was from 9 nm to 17 nm. Pure TiO₂ nanoparticles via BET studies showed surface area of 151 m²/g, whereas, TiO₂ nanoparticles doped with nitrogen and copper showed increased surface area between 253m²/g to 383 m²/g. Doped TiO₂ nanoparticles showed better photocatalytic activity for UV-Visible region for degradation of methylene blue and methyl orange [67].

2.4 Graphene oxide as a photocatalyst

Karthikeyan Krishnamoorthy, Rajneesh Mohan, and S. J. Kim (2011), reported the photocatalytic activity of graphene oxide. The synthesis of graphene oxide was done by altered hummers' technique and characterization techniques performed, confirmed the presence of oxygen groups on the surface of graphene sheets. The photocatalytic activity of graphene oxide was observed by reduction of resazurin into resorufin and their color was also changed from blue to pink. The reduction was done by the electrons present on the surface of graphene sheets when they were irradiated with UV light [68].

- **Hummers' method**

William S. Hummers, Jr. and Richard E. Offeman (1957), reported for the first time, the synthesis of graphite oxide by hummers' process. They prepared graphite oxide by adding graphite flakes and NaNO_3 to concentrated H_2SO_4 . The added mixture was kept in a battery jar that was kept at $0\text{ }^\circ\text{C}$ temperature under continuous stirring. KMnO_4 was then added slowly for oxidation of graphite. Temperature was then increased to $35\text{ }^\circ\text{C}$ for half hour. After that, addition of water was done slowly which caused the increase in temperature up to $98\text{ }^\circ\text{C}$. Addition of more water and then termination of reaction of H_2O_2 was done. Filtration and washing was done to separate the graphitic layers. Drying at $40\text{ }^\circ\text{C}$ was done to obtain powder form of graphite oxide. Large amount of graphite oxide was produced by this method [69].

Ji Chen, Bowen Yao, Chun Li and Gaoquan Shi (2013), introduced the eco-friendly method for the synthesis of graphene oxide by altering the already given hummers' process. They removed sodium nitrate from the conventional hummers' process to avoid the release of toxic and harmful gases. This process proved to be more eco-friendly as well as inexpensive and the process of cleansing the waste-water was made even easy. In this process, graphite flakes were added directly to sulfuric acid and continuous stirring was done in the presence of ice bath. Potassium permanganate was then added slowly for oxidation of graphene. Water was then added and reaction was terminated by hydrogen peroxide. Washing with hydrochloric acid and water done and then drying was done to obtain the graphene oxide sheets [70].

Leila Shahriary and Anjali A. Athawale (2014), reported the synthesis of graphene oxide sheets by altered hummers' process. This method involved addition concentrated sulfuric acid to graphite flakes and sodium nitrate mixed in a beaker with continuous stirring. Potassium permanganate was added after one hour for oxidation of graphene. This mixture was kept on stirring for 12 hours and then water was added to the mixture with same stirring but more vigorous. Hydrogen peroxide was added at the end to complete the reaction. Obtained mixture was treated with washing by hydrochloric acid and distilled water and drying of sheets was done [71].

Paulchamy B, Arthi G and Lignesh BD (2015), reported the synthesis of graphene oxide by hummers' process and altered hummers' process. This process involved the addition of NaNO_3 and H_2SO_4 to graphite powder under continuous stirring for 2 hours and kept at low temperature up to 5° . After 2 hours stirring, addition of KMnO_4 was done slowly and after that temperature was maintained to 35° and the solution is kept under stirring for 2 days. After 2 days stirring a grey slurry was formed, after which addition of water was done slowly and which was then moved to addition of H_2O_2 to terminate the reaction. The obtained solution is settled down and decanted, sonicated, washed with HCl and water and then dried in a vacuum oven for 24 hours to obtain graphene oxide. By different characterization techniques, especially XRD and FTIR analysis, oxygen functional group on graphene sheets' surface was confirmed. SEM images confirmed the exfoliation of graphite into graphene sheets [72].

2.5 Graphene oxide/ TiO_2 nanocomposite

N.R. Khalid, E. Ahmed and Zhanglian Hong (2012), reported the synthesis of nitrogen doped TiO_2 nanoparticles decorated on graphene oxide sheets via hydrothermal process. This work showed the increased photocatalytic activity for all the prepared nanocomposites as compared to bare TiO_2 nanoparticles for the degradation of methyl orange. When nitrogen doping was done and graphene oxide composites were formed as shown in **figure 2.5**, narrowing of bandgap occurred, electron-hole separation was seen and adsorptivity of methyl orange increased due to large specific surface area of graphene sheets [73].

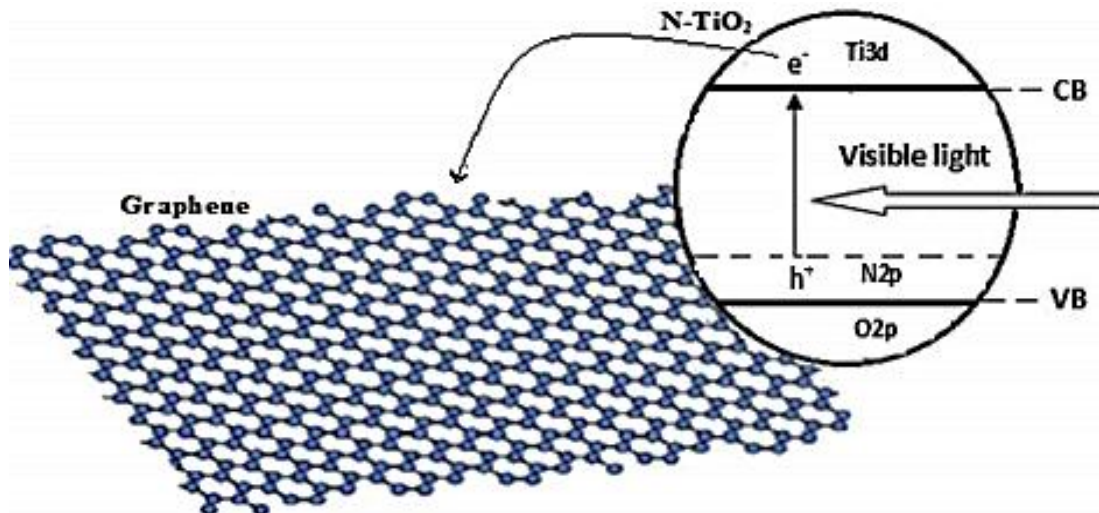


Figure 2.5 Scheme of photocatalytic activity of N-doped TiO₂/ GO composite

N. R. Khalid, E. Ahmed and Zhanglian Hong (2013), reported the synthesis of copper doped TiO₂ nanoparticles/ graphene oxide nanocomposite via hydrothermal process. Their photocatalytic activity studies showed the increased photoactivity for degradation of methyl orange in case of nanocomposite as compared to pure TiO₂ nanoparticles. The performance was improved due to electron-hole separation and increased adsorptivity of the nanocomposite due to sheet like structure of graphene oxide. The interaction of graphene oxide nanocomposite and the dye to be degraded was more, which confirmed the enhanced activity [74].

XiaopengShanga, Min Zhanga and Yingkui Yang (2014), reported the synthesis of sulphur and nitrogen co-doped TiO₂ nanoparticles/ graphene oxide nanocomposites by easy hydrothermal process. The nanocomposite prepared, showed enhanced photocatalytic activity when they were irradiated with UV light and used for the degradation of methyl orange. Graphene oxide because of its large specific surface area caused the increase in photocatalytic activity. Also, graphene oxide acts as a bridge for the transfer of electrons and reduces the risk of electron-hole recombination [75].

Hemraj M. Yadav and Jung-Sik Kim (2016), reported the synthesis of TiO₂ nanoparticles/ graphene oxide nanocomposites having various concentrations of graphene oxide via solvothermal process as shown in **figure 2.6**. Graphene oxide sheets were

identified by XRD data, TEM analysis and photoluminescence spectroscopy. Presence of TiO_2 nanoparticles on graphene oxide sheets was confirmed by SEM analysis. The composites prepared gave enhanced photocatalytic activity as compared to pure TiO_2 nanoparticles through degradation studies of benzene gas. This increased activity was because of the decreased charge recombination [76].

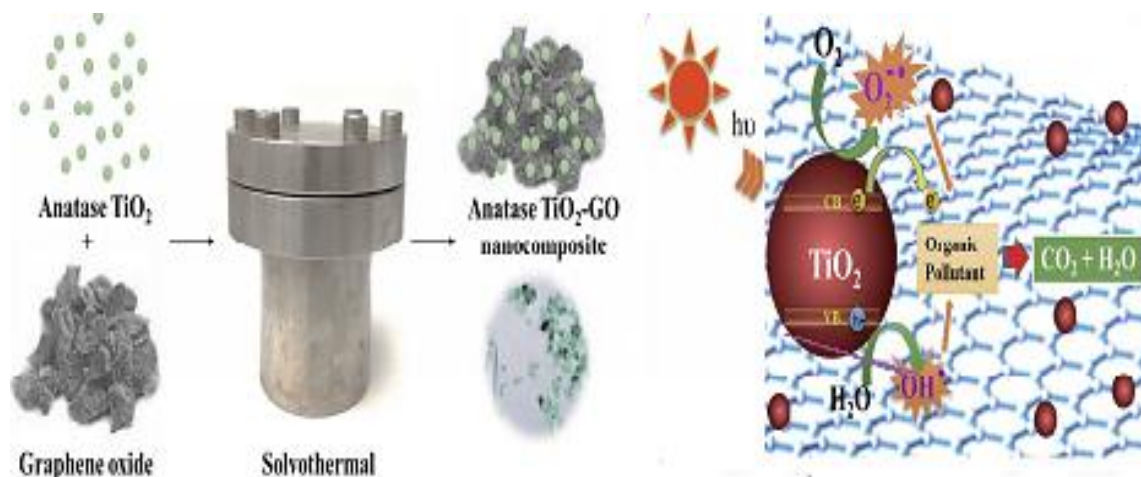


Figure 2.6 Schematic illustration of synthesis and photocatalysis of TiO_2/GO nanocomposite

3 EXPERIMENTAL WORK

This chapter covers the details of the chemicals and experimental procedure employed in this work. Furthermore, various characterization techniques used to analyze the sample have also been discussed briefly at the end of this chapter.

All chemicals used for the synthesis and preparation of desired catalysts and composites are of analytical grade and no further purification was required.

3.1 Synthesis of TiO₂ nanoparticles

Sol-gel method was used for the preparation of TiO₂ nanoparticles. Titanium (IV) isopropoxide (97%) was used as a precursor for TiO₂ and Urea was used as a precursor for nitrogen as a dopant.

3.1.1 Materials and chemicals

For synthesis of TiO₂ nanoparticles (bare, doped and co-doped), Titanium (IV) isopropoxide (97%) was purchased from Sigma Aldrich, Copper (II) nitrate trihydrate (Cu (NO₃)₂·3H₂O) (Sigma Aldrich), Urea (Merck) and Nitric acid and 2-propanol (Sigma Aldrich).

3.1.2 Procedure for synthesis of TiO₂ nanoparticles

For the synthesis of TiO₂ nanoparticles, 5 ml of Tetra Titanium isopropoxide (TTIP) was mixed with 6 ml of 2-propanol in a beaker and stirred for 15 min. In another beaker, 2-3 drops of nitric acid were added in 80 ml of water to bring the pH to 3. The previous prepared solution of TTIP and 2-propanol was then drop-wise added to this water under vigorous continuous stirring. This solution was then stirred overnight. This solution after one night was then dried in vacuum oven for 8 h under 80 °C temperature. The obtained dried solid particles were then ground in to fine powder. This powder was further annealed at 450 °C for 8 h to obtain anatase form of TiO₂ nanoparticles in white powder form.

Nitrogen and copper doping was done similarly by the same process. Nitrogen percentage was kept same as was reported in literature but copper concentrations were varied.

3.1.3 Procedure for synthesis of nitrogen doped TiO₂ nanoparticles

For nitrogen doping 3 g of urea was added in water that was containing 2-3 drops of nitric acid and then drop wise addition of TTIP and 2-propanol was done. The mixture was stirred overnight, dried under vacuum at 80 °C for 8 h and annealed at 450 °C and yellowish powder was obtained.

3.1.4 Procedure for synthesis of copper and nitrogen co-doped TiO₂ nanoparticles

For nitrogen and copper co-doping, 3 g of urea with 0.1%, 0.5%, 1%, 2% and 3% copper nitrate trihydrate was added separately in water containing nitric acid and 5 solutions were prepared. Drop-wise addition, stirring overnight, drying at 80 °C and annealing at 450 °C was done and light blue to green colored powder were obtained depending upon the percentage of copper being used. Given in **figure 3.1** are the processes that were performed while preparation of TiO₂ nanoparticles.



Figure 3.1(a) TTIP + propanol solution, (b) Drop-wise addition to H₂O+HNO₃ solution

The left figure is taken after 15 min stirring of TTIP and 2-propanol solution and the right figure shows the addition of as prepared solution of TTIP and 2-propanol to H₂O containing few drops of HNO₃.

In **figure 3.2**, it can be seen in the second figure that solution of water containing 3 % of $\text{Cu}(\text{NO}_3)_2 \cdot 3\text{H}_2\text{O}$ has a change in its color. Similarly, the products obtained before annealing or after annealing have different color transitions. Also the colors of different samples with different percentages are also varying according to the amount of Cu percentage.

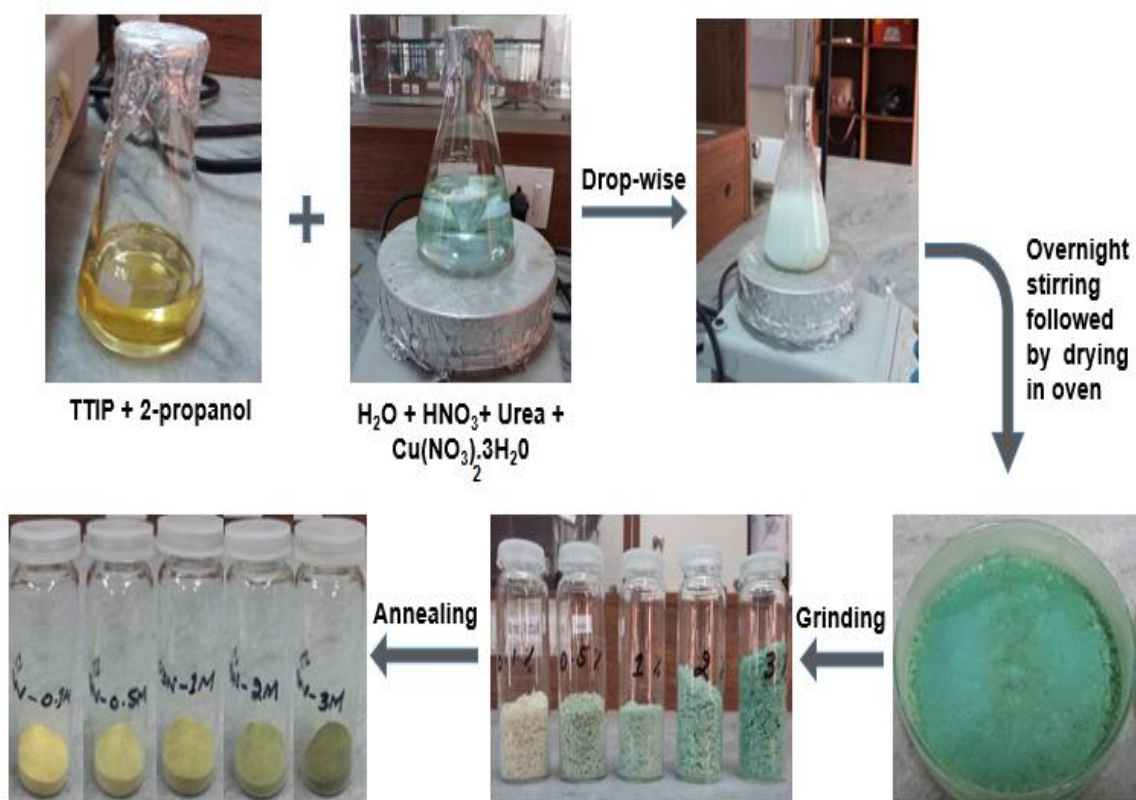


Figure 3.2 Schematic illustration for the preparation of Cu/N co-doped TiO_2 nanoparticles

3.2 Synthesis of graphene oxide

Hummers' method was used for the synthesis of graphene oxide nanosheets. Graphite powder was used as a precursor for graphene oxide.

3.2.1 Materials and chemicals

Graphite powder (Sigma Aldrich), Sodium Nitrate (BDH), Potassium permanganate (Sigma Aldrich), Hydrogen peroxide (Merck), Sulfuric acid (95 %) (Sigma Aldrich), Hydrochloric acid (37 %) (Sigma Aldrich).

3.2.2 Procedure for graphene oxide synthesis

For graphene oxide nanosheets synthesis, 2 g of graphite flakes in 1000 ml beaker were taken, 50 ml of H_2SO_4 (98 %) was added in it and reaction mixture was kept at 0-5 °C in ice bath under continuous stirring. To create defects, 2 g of NaNO_3 was added slowly. The reaction mixture was stirred at 0-5 °C for 2 h. To oxidize graphite flakes 6 g of KMnO_4 was added slowly and kept at max 15 °C temperature.

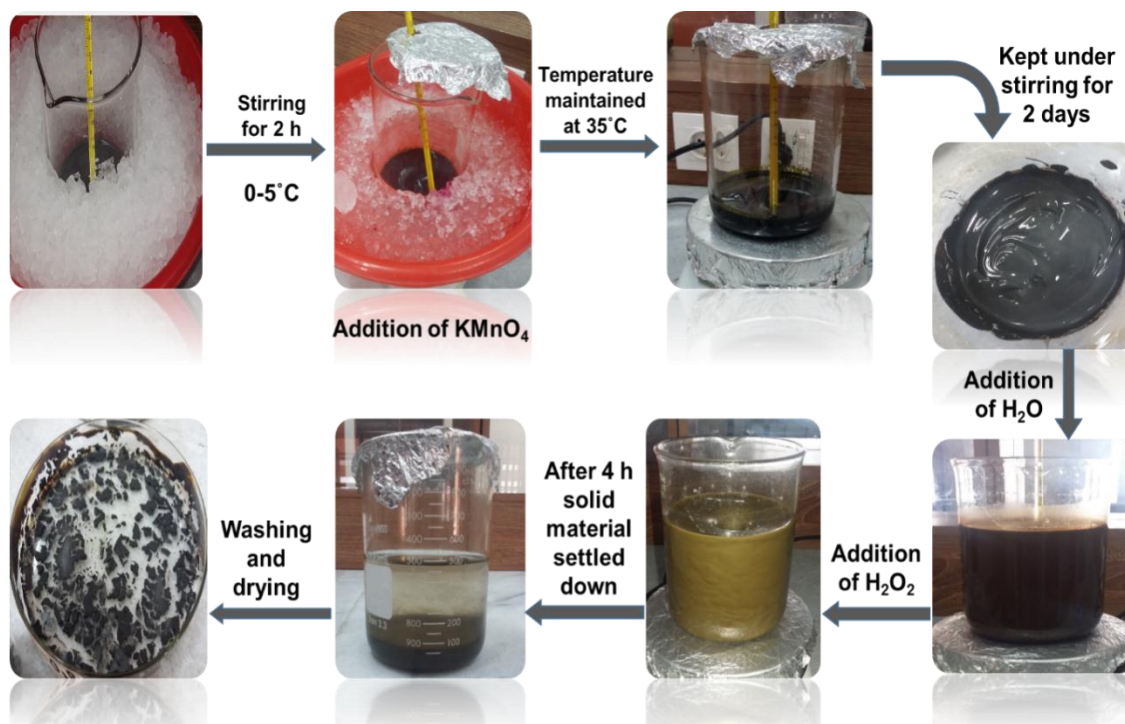


Figure 3.3 Schematic illustration of synthesis of graphene oxide

The ice bath was then removed, temperature was maintained at 35 °C and the resultant brownish mixture was stirred for 2 days. Slow addition of 100 ml of H_2O was done to dilute reaction mixture. Rapid increase in reaction temperature (up to 98 °C) appeared with effervescence. Addition of water changes the color of slurry from grey to brown. Under continuous stirring, the reaction mixture was further diluted with 200 ml of H_2O . To terminate the reaction, drop-wise addition of 10 ml of H_2O_2 was done that gave yellow color to the reaction mixture. The reaction mixture was then washed with 10 % HCl and several times with deionized water until pH 7 was achieved. The obtained gel like material

was then dried in vacuum oven at 60 °C to obtain GO powder. Schematic illustration of synthesis of graphene oxide can be seen in **figure 3.3**.

3.3 Synthesis of GO/Cu-N co-doped TiO₂ nanocomposite

After the degradation study of dye by using co-doped TiO₂, we selected the best catalyst and prepared its nanocomposite with already prepared GO to further enhance the photocatalytic properties and check its degradation capability. Hydrothermal method was used for their preparation.

3.3.1 Chemicals and materials

As prepared best selected nitrogen and copper co-doped TiO₂ nanoparticles and graphene oxide.

3.3.2 Procedure

Three ratios of GO/TNPs were taken to study the degradation of dye. Graphene oxide (0.5:1, 1:1 and 2:1) was dispersed in 30 ml of deionized water by probe sonicator separately in 3 different beakers.

After 30 minutes of sonication same amount of best selected co-doped TiO₂ nanoparticles powder was added in to each of the three beakers and again sonication was done at low amplitude. Then vigorous stirring was done for 3 hours. The prepared suspensions were transferred to autoclaves and held at 120 °C for 4 hours. The products obtained were then washed with deionized water several times and dried under vacuum at 60 °C. Powder form of samples was obtained as shown in **figure 3.4**.



Figure 3.4 Prepared GO/Cu-N co-doped TiO₂ nanocomposites

Table 3.1 Details of TiO₂ and doped-TiO₂ photocatalysts

Sample ID	Composition	Dopant %age	Annealing Temp.
T	TiO ₂	0%	450 °C
NT	Nitrogen doped TiO ₂	3%-N	450 °C
0.1%Cu-NT	Copper and Nitrogen co-doped TiO ₂	3%-N, 0.1%-Cu	450 °C
0.5%Cu-NT	Copper and Nitrogen co-doped TiO ₂	3%-N, 0.5%-Cu	450 °C
1%Cu-NT	Copper and Nitrogen co-doped TiO ₂	3%-N, 1%-Cu	450 °C
2%Cu-NT	Copper and Nitrogen co-doped TiO ₂	3%-N, 2%-Cu	450 °C
3%Cu-NT	Copper and Nitrogen co-doped TiO ₂	3%-N, 3%-Cu	450 °C

Table 3.2 Details of GO/TiO₂ nanocomposites

Sample ID	Composition	Amounts
0.5:1-GO/T	Graphene Oxide, Copper and Nitrogen co-doped TiO ₂	125mg GO, 250mg 2% Cu-NT
1:1-GO/T	Graphene Oxide, Copper and Nitrogen co-doped TiO ₂	250 mg GO, 250mg 2% Cu-NT
2:1-GO/T	Graphene Oxide, Copper and Nitrogen co-doped TiO ₂	500 mg GO, 250mg 2% Cu-NT

4 RESULTS AND DISCUSSION

This chapter includes all the characterization techniques performed and all the results concluded from different studies.

4.1 Structural and morphological analysis

Structural analysis of all the prepared samples was done by X-ray Diffraction (XRD) data, Scanning Electron Microscopy (SEM) analysis, Energy Dispersive X-ray Spectroscopy (EDS) data, Fourier Transform Infrared Spectroscopy (FTIR) absorption frequencies and UV/Visible-DRS data.

4.1.1 XRD

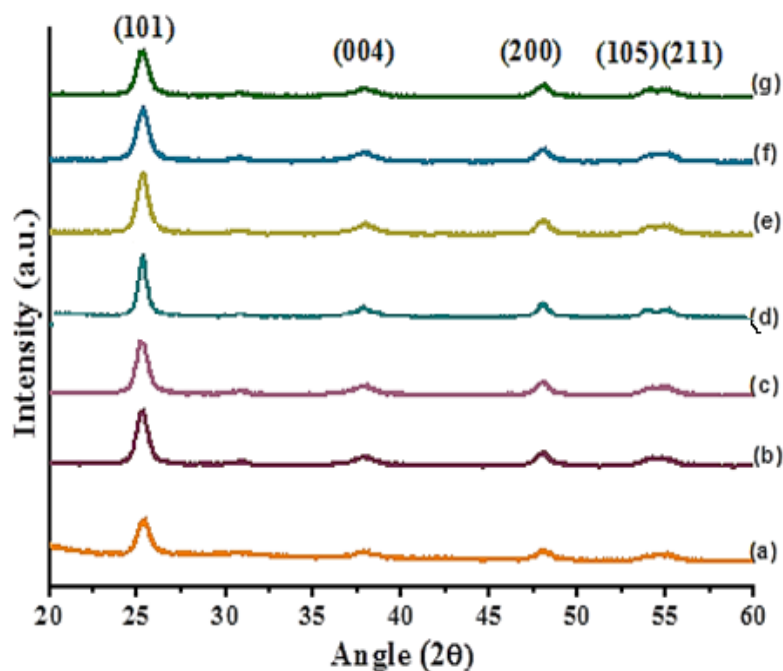


Figure 4.1 XRD peaks of prepared nanoparticles showing: (a) Pure TiO₂ (b) N- TiO₂ (c) 0.1% Cu-NT (d) 0.5% Cu-NT (e) 1% Cu-NT (f) 2% Cu-NT (g) 3% Cu-NT

XRD machine used for this study was JSX 3201, Jeol, Japan present at School of Chemical and Material Engineering, NUST, Islamabad. JCPDS No.21-1272 clearly matches with all the obtained XRD results of prepared nanoparticles and the absence of impurity peaks also confirms phase purity. TiO₂ anatase is in highly crystalline form which can be observed from narrow and Sharpe peaks. Diffraction peaks appeared at

25.30°, 37.82°, 42.14, 48.01°, 53.97° and 55.06° having lattice planes at (101), (004), (200), (105) and (211) respectively. The dopant elements nitrogen and copper do not show peaks because of low concentration but a slight shift of peaks due to doping can be seen in **figure 4.1** and clearly in **table 4.1**. This is because of incorporation of Cu and N ions into TiO₂ lattice that causes a change in cell volume and cell parameters of TiO₂ crystal lattice. Characteristic rutile peaks were not observed as pure anatase phase was formed and is confirmed.

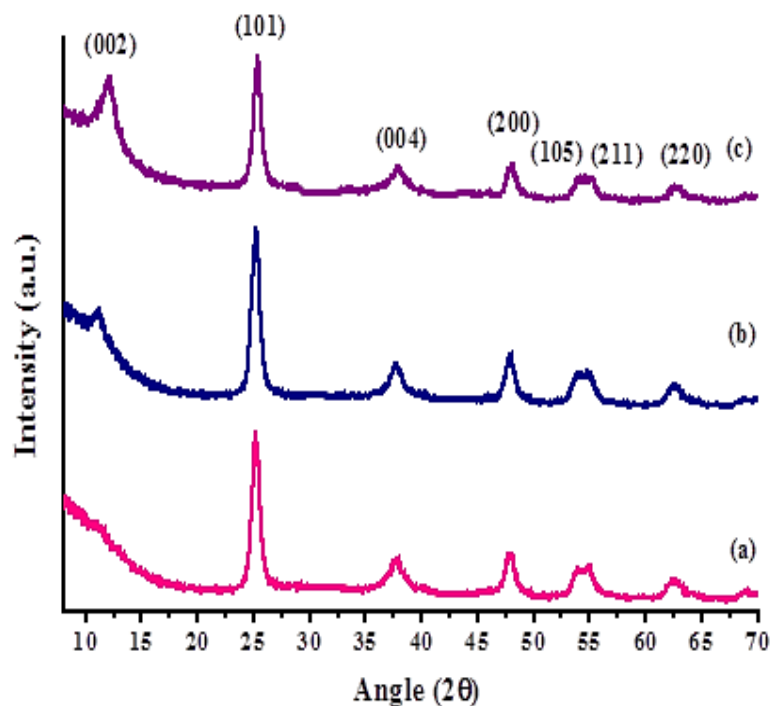


Figure 4.2 XRD peaks of prepared nanocomposites showing: (a) 0.5:1 GO-T (b) 1:1 GO-T (c) 2:1 GO-T

In **figure 4.1**, the anatase phase of 2% Cu/N co-doped TiO₂ nanoparticles can be clearly seen and the crystallinity of the samples can be confirmed by increased intensity of peaks and decreased broadening. Moreover, this figure shows the results of the nanocomposites GO and the prepared catalyst with different ratios (0.5:1, 1:1 and 2:1). The characteristic peak of GO which appears at 10.7° having lattice plane at (002), can be seen in all the composites with increase in intensity by increasing the concentration of GO. The peaks are also shifted from their position due to composite formation.

Average crystallite size of all the prepared catalysts was calculated by Scherrer equation:

$$D = k\lambda / \beta \cos\theta$$

Where,

D = Crystallite size

k = Scherrer constant

It is a shape factor and its value is close to unity but varies with shape of crystallite.

λ = Wavelength of x-rays used (Cu k-alpha are mostly used having wavelength of 0.15405 nm)

β = Full width half maximum (FWHM) of observed peak

θ = Diffraction angle in degrees

Pure TiO₂ has crystallite size of 20 nm and doping lowers the size up to 11 nm. This lowering of crystallite size with increase in dopant concentration can be clearly observed in **table 4.1**.

Table 4.1 Average crystallite size of all prepared catalysts and composites

Sample ID	Peak Position	FWHM	Crystallite size of peak (nm)	Average crystallite size (nm)
T	25.30	0.39	25.9	20.9
	37.82	0.39	26.7	
	48.01	0.47	22.2	
	53.97	0.55	18.9	
	55.06	0.48	22.4	
NT	25.34	0.39	25.9	16.1
	37.91	0.94	9.7	
	48.05	0.55	18.5	
	54.02	0.47	22.7	
	55.15	0.63	16.3	
0.1%Cu-NT	25.41	0.70	12.9	16.1
	37.96	0.47	21.4	
	48.05	0.63	15.8	
	54.03	0.55	18.9	

	55.19	0.76	13.0	
0.5%Cu-NT	25.42	0.70	13.0	15.1
	37.98	0.63	15.3	
	48.06	0.70	13.8	
	54.05	0.47	22.7	
	55.20	0.76	13.0	
1%Cu-NT	25.42	0.63	14.8	14.4
	37.95	0.70	13.4	
	48.16	0.70	13.8	
	54.10	0.47	22.7	
	55.23	0.86	11.5	
2%Cu-NT	25.43	0.55	17.3	13.7
	37.98	0.62	15.3	
	48.20	0.62	15.8	
	54.09	0.62	16.2	
	55.28	0.96	10.2	
3%Cu-NT	25.42	0.76	11.8	11.7
	37.98	0.76	12.2	
	48.20	0.86	11.1	
	54.15	0.67	15.0	
	54.34	0.96	10.2	
0.5:1 GO-T	11.31	0.94	8.5	13.7
	25.46	0.63	13.1	
	37.98	0.55	15.5	
	48.20	0.70	12.4	
	54.07	0.47	19.2	
	55.28	0.39	23.2	
1:1 GO-T	11.14	0.47	17.2	13.6
	25.44	0.70	11.6	
	37.90	0.63	13.5	
	48.21	0.63	14.0	
	54.09	0.70	12.7	

	55.24	0.63	14.4	
2:1 GO-T	12.13	0.39	20.7	13.3
	25.45	0.63	13.1	
	37.96	0.78	10.8	
	48.27	0.78	11.2	
	54.13	0.63	14.3	
	55.26	0.94	9.6	

4.1.2 SEM

SEM used in this study for the characterization of sample is JSM-6490A, JEOL-Japan, present at School of Chemical and Materials Engineering, NUST, Islamabad. The morphology of pure TiO₂ was spherical but the doped particle become more like aggregated plates. Agglomeration was also seen in samples that were probably because of nucleation during hydrolysis or heat treatment.

Cu doping affects the catalyst by decreasing grain size and in turn increasing the surface area which leads to increased photocatalytic activity. **Figure 4.3** shows spherical morphology of all the prepared catalysts and increase in agglomeration with increase in copper content. Copper plates can also be seen in the prepared catalysts, especially is 3% Cu/N co-doped TiO₂ nanoparticles as it contains the highest amount of copper.

Table 4.2 Average particle size of all prepared samples

Sample ID	Average particle size (nm)	Sample ID	Average particle size (nm)
T	36.33	2%Cu-NT	18.48
NT	33.92	3%Cu-NT	14.18
0.1%Cu-NT	32.17	0.5:1-GO/T	18.39
0.5%Cu-NT	30.35	1:1-GO/T	19.74
1%Cu-NT	29.78	2:1-GO/T	16.72

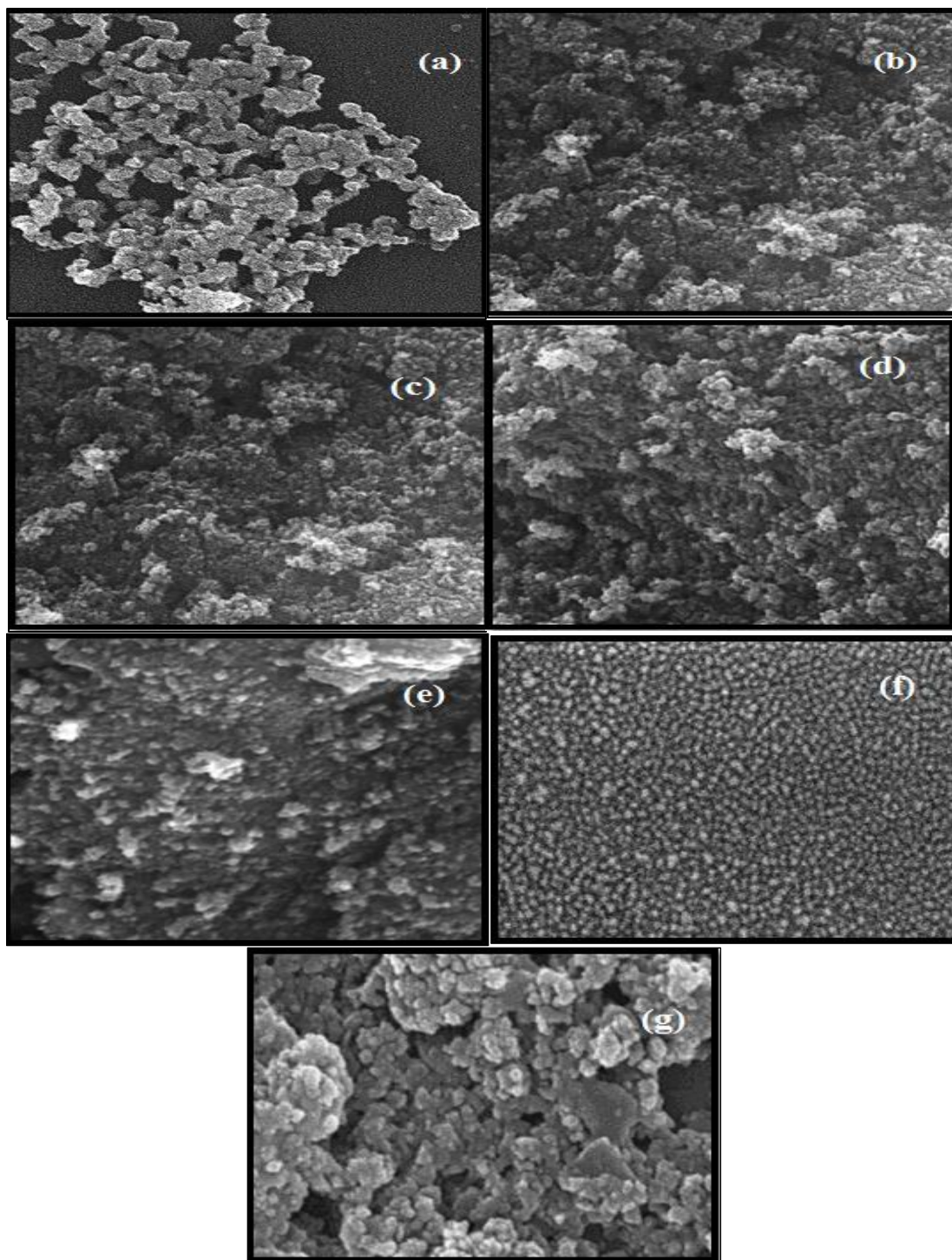


Figure 4.3 SEM images: (a) Pure TiO₂ (b) N- TiO₂ (c) 0.1% Cu-NT (d) 0.5% Cu-NT (e) 1% Cu-NT (f) 2% Cu-NT (g) 3% Cu-NT

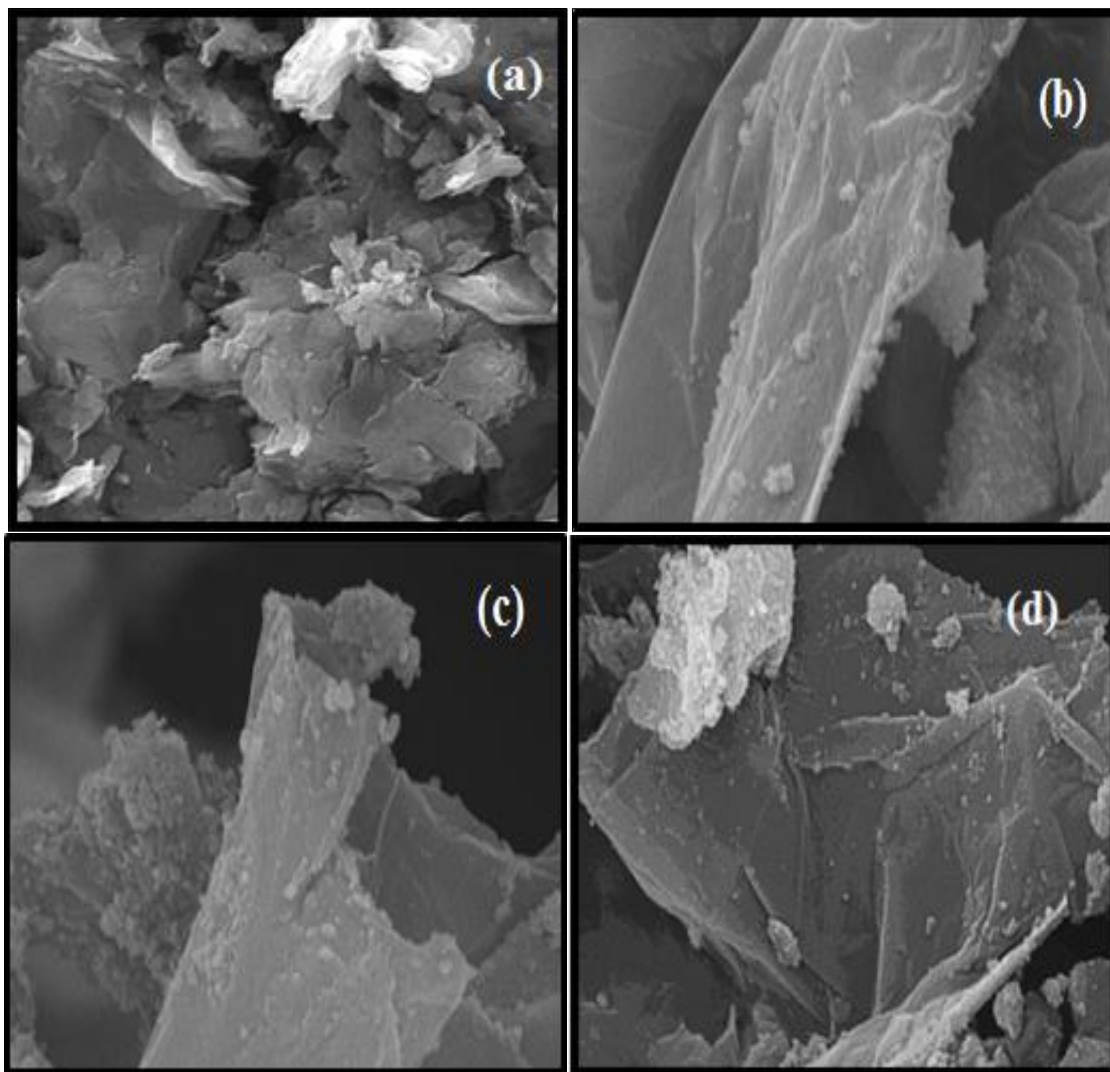


Figure 4.4 SEM images: (a) GO (b) 0.5:1 GO-T (c) 1:1 GO-T (d) 2:1 GO-T

SEM images of graphene oxide show stacked sheets as shown in **Figure 4.4 (a)**. These sheets are of micrometer size and may have thickness in nanometer range depending on the number of stacked sheets. **Figure 4.4 (b), (c) and (d)** shows incorporation of 2% Cu/N co-doped TiO_2 nanoparticles on GO sheets. The particle size of all the prepared catalysts and composites is shown in **table 4.2** and it can be seen that increase in dopant concentration has decreased the particle size from 36 nm to 14 nm.

4.1.3 EDS/EDX

EDS or EDX is used for the elemental composition detection of the sample. Each element show specific peak in the graph depicting its presence in the sample. TESCAN machine present at USP-CASE, NUST was used for EDX analysis. **Figure 4.5** shows EDX analysis of all the prepared catalysts. There is no copper content in pure TiO_2 and in N- TiO_2 and it is clearly seen in **figure 4.5 (a)** and **(b)** that only peak of Ti and O are present and N due to its less weight does not show its peak. But copper peaks are clearly seen in **figure 4.5 (c)**, **(d)**, **(e)**, **(f)** and **(g)** according to their concentrations along with Ti and O peaks.

EDS results obtained for each prepared sample exactly shows the amount of each element that is either already present or is doped. The amount of copper that is varied from 0.1% to 2% is clearly seen in the weight percentages in **table 4.3**. Whereas, there are no peaks observed for copper in the case of pure TiO_2 and N-doped TiO_2 . There is also a slight peak of gold observed in all the results because gold studs were used for sample analysis. Nitrogen content cannot be seen in each sample as the weight of nitrogen is very low and its amount cannot be observed.

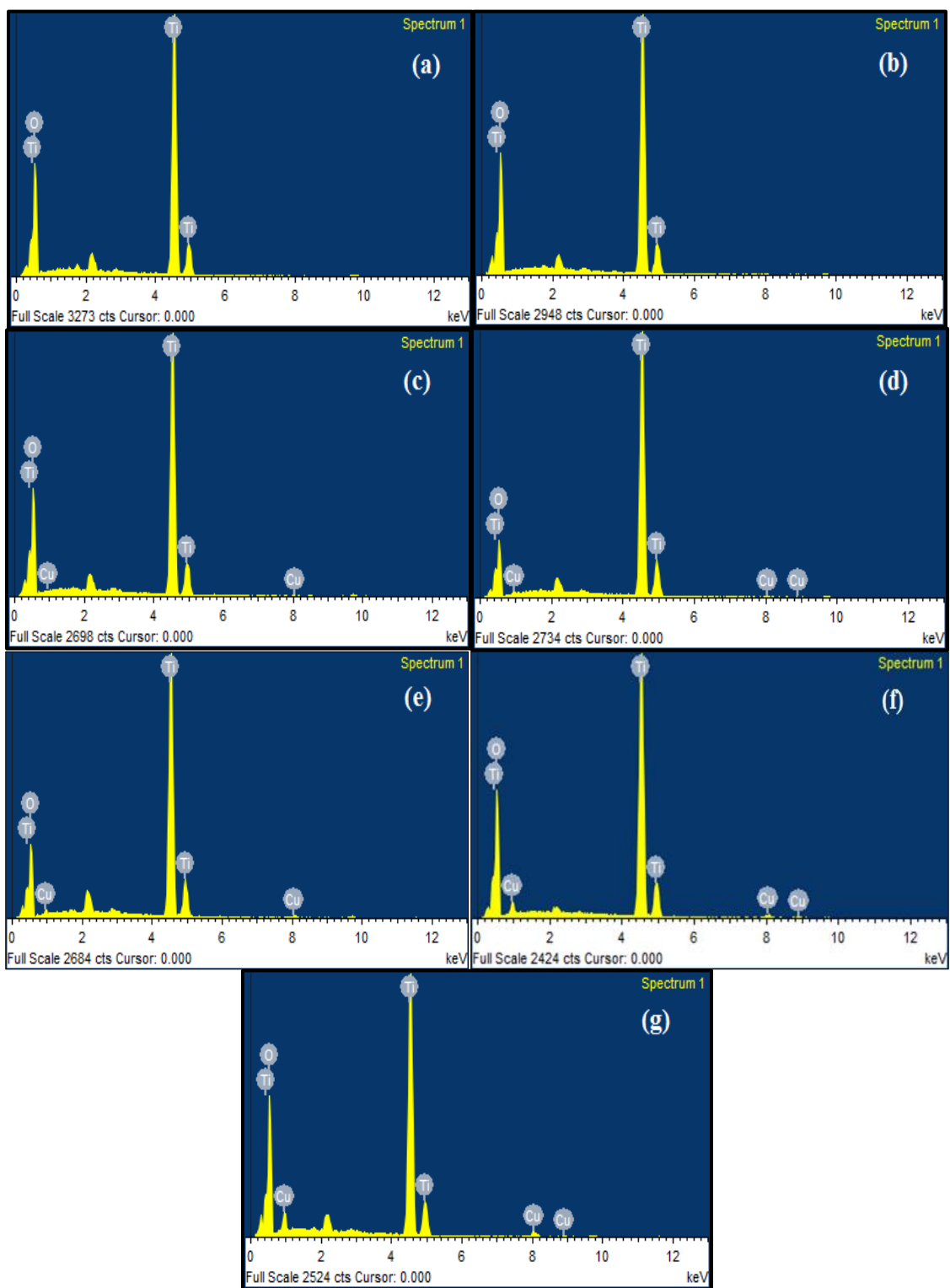


Figure 4.5 EDS analysis: (a) Pure TiO₂ (b) N- TiO₂ (c) 0.1% Cu-NT (d) 0.5% Cu-NT (e) 1% Cu-NT (f) 2% Cu-NT (g) 3% Cu-NT

Table 4.3 EDS results: (a) Pure TiO₂ (b) N- TiO₂ (c) 0.1% Cu-NT (d) 0.5% Cu-NT (e) 1% Cu-NT (f) 2% Cu-NT (g) 3% Cu-NT

Element	Weight%	Atomic%	Element	Weight%	Atomic%
O K	68.03	86.44	O K	69.22	87.07
Ti K	31.97	13.56	Ti K	30.78	12.93
Totals	100.00	(a)	Totals	100.00	(b)

Element	Weight%	Atomic%	Element	Weight%	Atomic%
O K	63.34	83.82	O K	58.57	80.94
Ti K	36.51	16.13	Ti K	40.85	18.86
Cu K	0.15	0.05	Cu K	0.58	0.20
Totals	100.00	(c)	Totals	100.00	(d)

Element	Weight%	Atomic%	Element	Weight%	Atomic%
O K	61.15	82.58	O K	69.21	87.25
Ti K	37.93	17.11	Ti K	28.73	12.10
Cu K	0.92	0.31	Cu K	2.06	0.65
Totals	100.00	(e)	Totals	100.00	(f)

Element	Weight%	Atomic%
O K	29.53	55.92
Ti K	67.30	42.57
Cu K	3.17	1.51
Totals	100.00	(g)

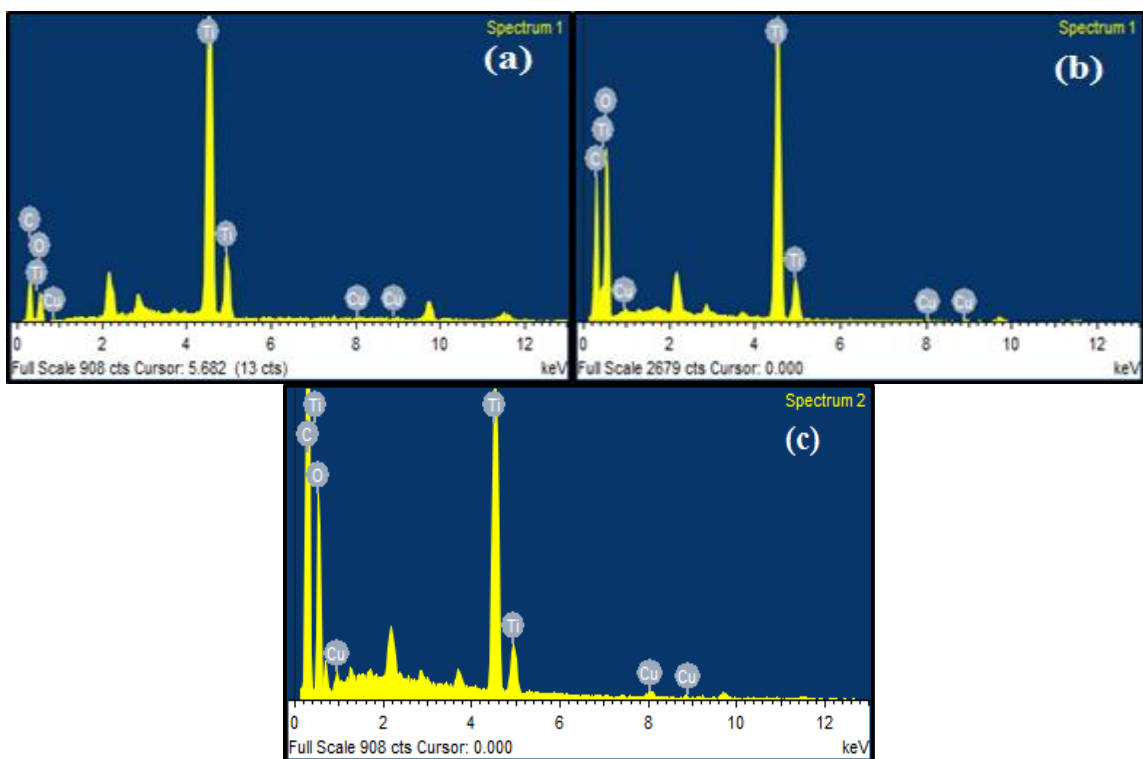


Figure 4.6 EDS analysis: (a) 0.5:1 GO-T (b) 1:1 GO-T (c) 2:1 GO-T

Table 4.4 EDS results of: (a) 0.5:1 GO-T (b) 1:1 GO-T (c) 2:1 GO-T

Element	Weight%	Atomic%	Element	Weight%	Atomic%
C K	24.48	42.55	C K	31.12	42.11
O K	28.28	36.90	O K	51.04	51.85
Ti K	46.86	20.42	Ti K	17.59	5.97
Cu K	0.38	0.12	Cu K	0.26	0.07
Totals	100.00	(a)	Totals	100.00	(b)

Element	Weight%	Atomic%
C K	61.53	71.63
O K	29.51	25.79
Ti K	8.49	2.48
Cu K	0.48	0.11
Totals	100.00	(c)

Moving towards the results of nanocomposites, EDS analysis in **figure 4.6** shows the presence of Ti, O, Cu and C content in each prepared sample. The prepared samples contained 2% Cu/N co-doped TiO₂ and GO with various ratios of GO (0.5, 1 and 2) and constant amount of catalyst. This can be clearly seen in the figure as the carbon content is increasing with increase in the ratio of GO. This illustrates the correct composite formation. For the confirmation of these results and the increase in carbon content, the results in **table 4.4** easily show the evidence.

4.1.4 FT-IR

FT-IR spectra of all prepared composites and GO are present in **figure 4.7**. The TiO₂ range in IR is from 450 cm⁻¹ to 200 cm⁻¹, and the instrument used for FTIR is ALPHA model, SN 200488 present in SNS, NUST in Islamabad, which has range from 4000 to 500 cm⁻¹. Still, a prominent peak at 500 cm⁻¹ is seen in all composites which were because of stretching vibrations of Ti-O-Ti bonds. Peaks at 3224 and 1387 cm⁻¹ are because of the stretching and bending vibrations of adsorbed water molecules, respectively, which are present in GO and TiO₂ both.

GO has many oxygen containing functional groups attached that's why it shows many characteristic peaks. Broad peak at 3200 -3500 cm⁻¹ is representing stretching vibrations of -OH bond, peak at 1722 cm⁻¹ is because of -C=O stretching and prominent peak at 1622 cm⁻¹ is because of C=C stretching vibrations.

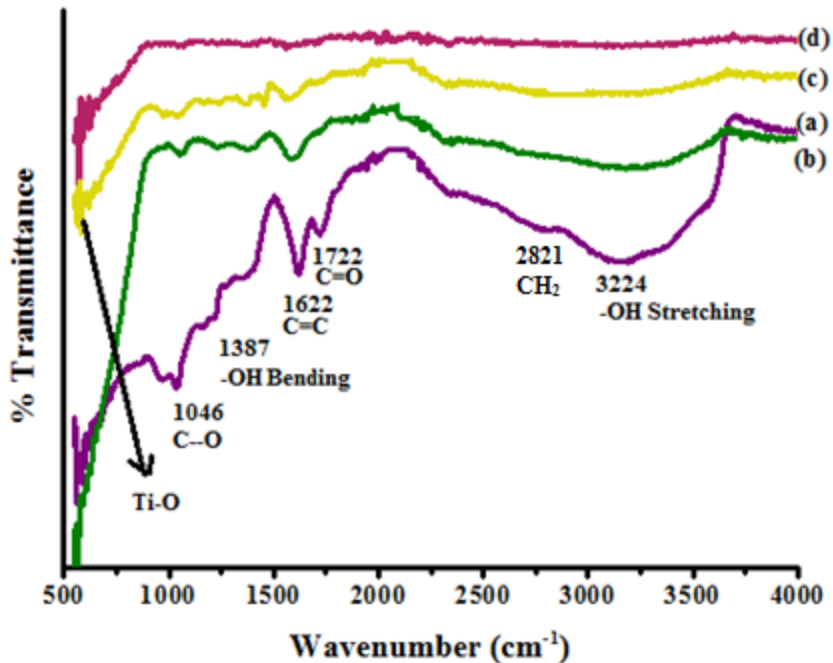


Figure 4.7 FT-IR spectra of (a) GO (b) 0.5:1 GO-T (c) 1:1 GO-T (d) 2:1 GO-T

4.1.5 UV/visible DRS

Tauc plots were formed from absorbance which was calculated using wavelength obtained from the DRS data using the equation:

$$E = h\nu/\lambda$$

$$\text{As } 1 \text{ eV} = 1.60 \times 10^{-19} \text{ J}$$

$$h\nu = (6.62 \times 10^{-34} \text{ Js}) \cdot (3 \times 10^8 \text{ m/s})$$

$$h\nu = 6.62 \times 10^{-34} \cdot (1.6 \times 10^{-19}) (3 \times 10^8 \text{ m/s})$$

$$h\nu = 1.24 \text{ eV} \times 10^{-6} = 1240 \text{ V nm}$$

$$h\nu = 1240/\lambda = \text{band gap in eV}$$

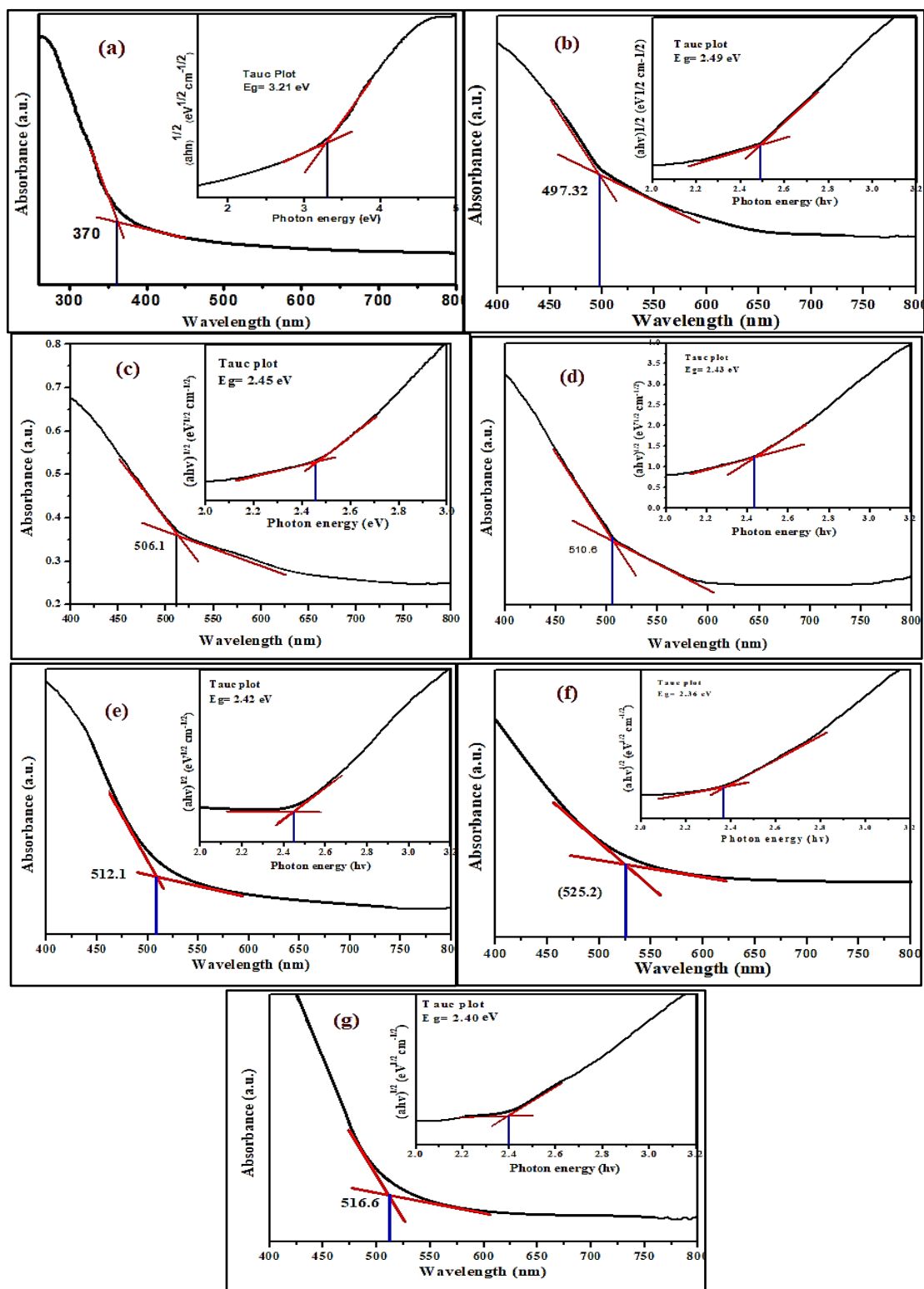


Figure 4.8 Absorbance and Tauc plots of: (a) T (b) NT (c) 0.1%-NT (d) 0.5%-NT (e) 1%-NT (f) 2%-NT (g) 3%-NT

The tauc plots data evaluated and showed the bandgap reduction in the entire prepared sample with increase amount of Cu content. It can be seen in **figure 4.8** that 2% Cu/N co-doped TiO₂ show most decreased bandgap of 2.36 eV.

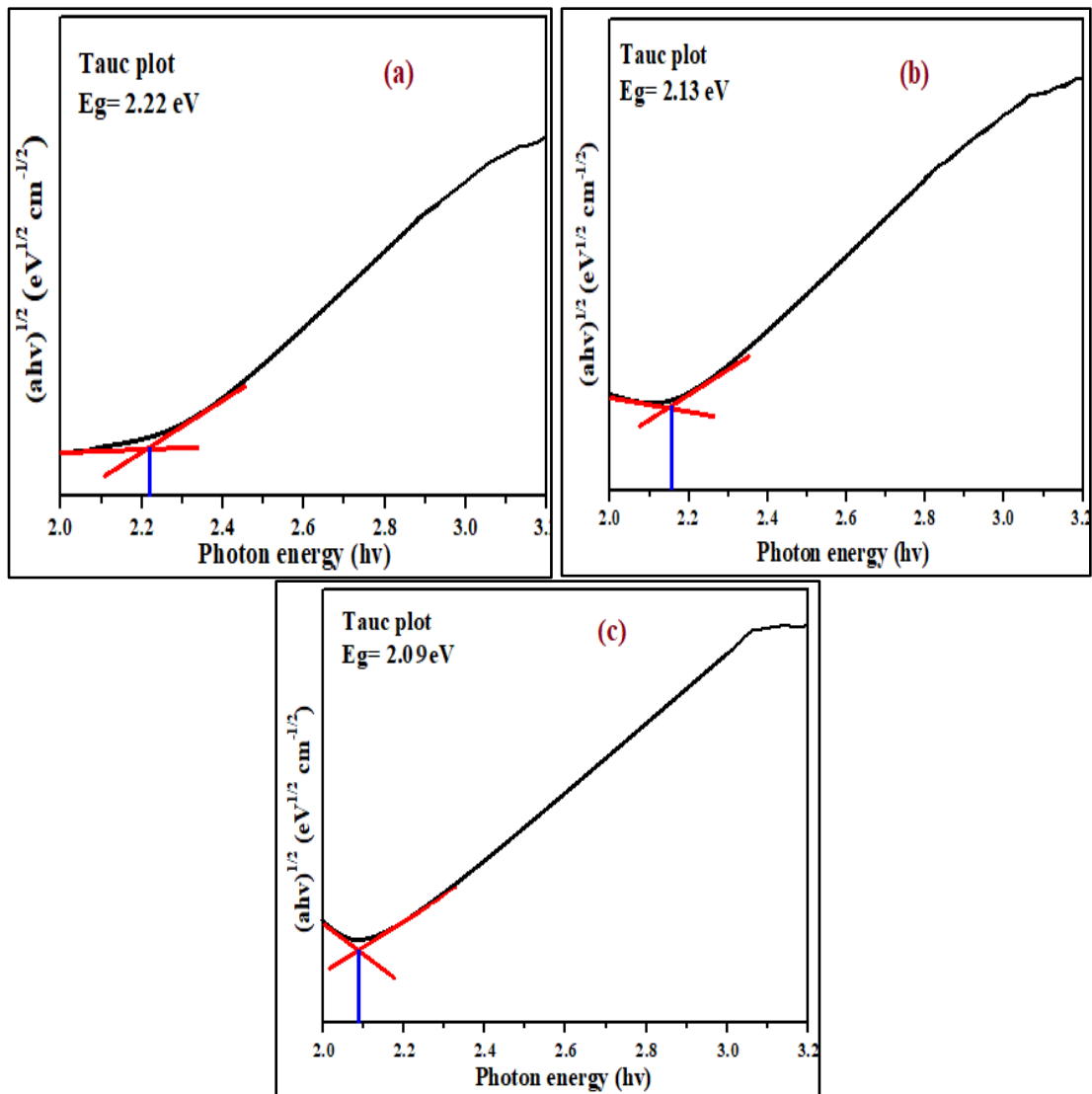


Figure 4.9 Tauc plots of: (a) 0.5:1 GO-T (b) 1:1 GO-T (c) 2:1 GO-T

Figure 4.9 shows all the tauc plots for prepared composites and it can be seen that the bandgap is reduced to 2.09 in case of the highest concentration of GO composite. This clearly illustrates that band gap is reduced when doping was done and it is further reduced when composites were formed.

The band gaps of all the prepared samples obtained from DRS data are shown in **table 4.5** and their decrease trend can be easily seen for all the samples.

Table 4.5 Bandgaps of all prepared samples

Sample ID	Band-gap (eV)	Sample ID	Band-gap (eV)
T	3.21	2%-NT	2.36
NT	2.49	3%-NT	2.40
0.1%-NT	2.45	0.5:1 GO-T	2.22
0.5%-NT	2.43	1:1 GO-T	2.13
1%-NT	2.42	2:1 GO-T	2.09

4.2 Degradation studies

To apply the optical properties of prepared nanocatalysts and nanocomposites, degradation studies were carried out on methyl orange. For this study, a stock solution of 3 mM for methyl orange was made, from which first 0.1 mM solution was obtained and then a more dilute 0.01 mM solution was obtained on which degradation studies were carried out for all the prepared samples.

First the study of all the prepared catalysts was done and the catalyst showing the best efficiency was then combined with GO to achieve extra efficiency. For catalysts study, a solution of 50 mg of each catalyst and 0.01 mM of methyl orange was prepared separately in 50 ml volumetric flasks and was kept in dark for 2 hours to attain adsorption-desorption equilibrium. After 2 hours stirring in dark, samples were kept in the reactor chamber under 250 W energy savers and with continuous shaking over a shaker at 160 rpm. 5 ml of each solution was taken out after different intervals of time which was then centrifuged for 3 minutes at 10000 rpm to let the catalyst settle down. The solution other than the catalyst was examined from a UV-Visible spectrophotometer to study the photocatalytic activity and the level of degradation. MO have characteristic peak at 464 nm and decrease in the absorbance at this point indicates MO degradation.

It was observed from the degradation studies that all doped samples show more degradation than un-doped or pure TiO₂ and when doped samples were compared with each other 2% Cu/N co-doped TiO₂ showed best photocatalytic activity. The degradation rate was decreased further for 3% Cu/N co-doped TiO₂. The reason for decreased photocatalytic activity can be the production of CuO and CuO₂, which was then deposited on the surface of the catalyst and caused less sunlight to reach the surface of the catalyst.

Degradation also depends upon the number of hydroxyl radicals. Excess amount of Cu^{2+} ions react with hydroxyl radicals and as a result $\{\text{Cu}(\text{H}_2\text{O})\}^{n+1}$ is formed, hence decreasing the photocatalytic activity.

In **figure 4.10**, all the degradation spectra are shown for each prepared catalyst and the best results can be seen for the 2% Cu/N co-doped TiO_2 photocatalyst as the degradation rate is very high for that catalyst. The best sample showed degradation in 5 hours up to 93% which was only 59% in the case of pure TiO_2 .

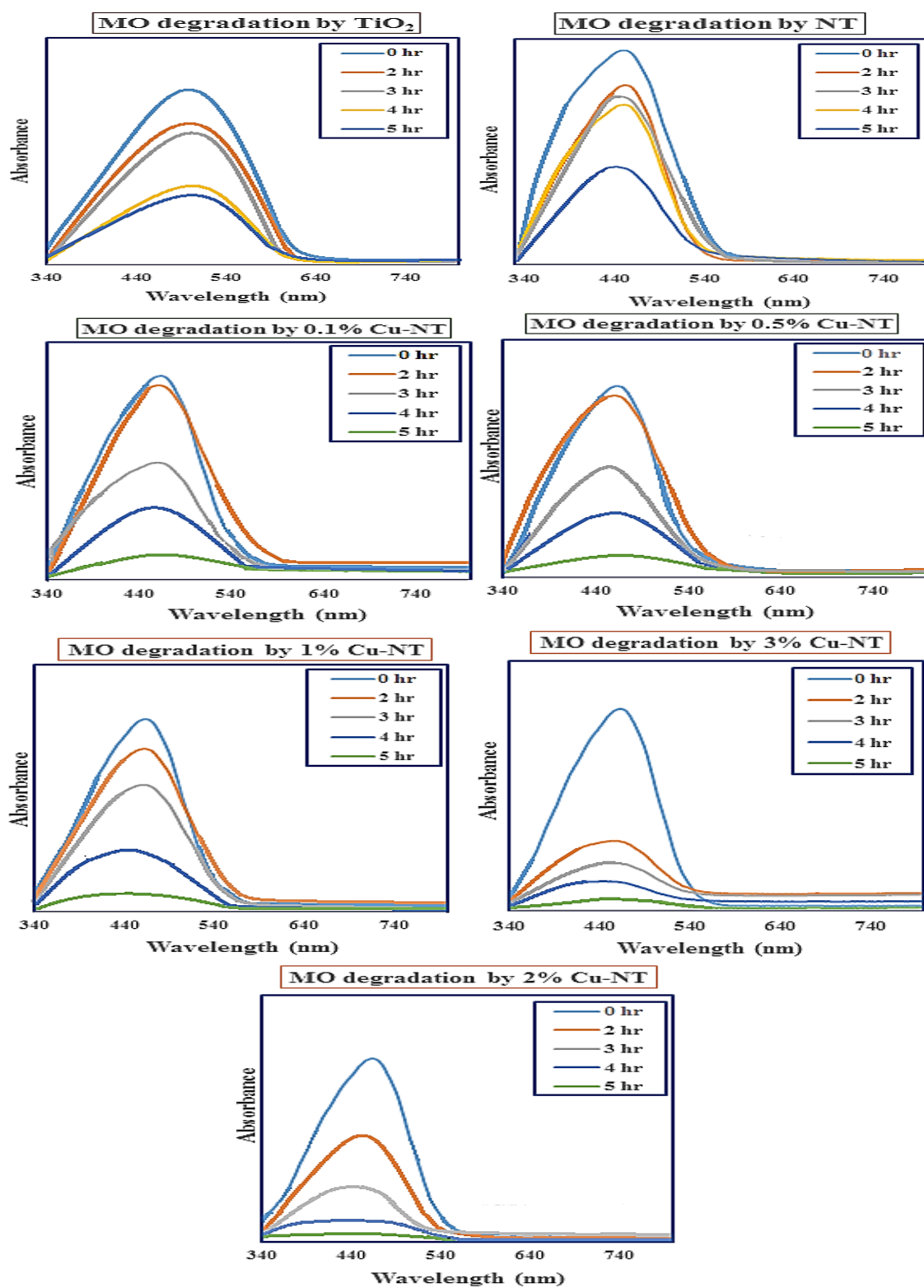


Figure 4.10 Degradation spectra of methyl orange using all prepared photocatalysts

Table 4.6 Degradation rate calculations for MO degradation using all catalysts under visible light irradiation

Catalyst	Time (hr)	Absorbance			Average	C_t	C_o	C_t/C_o	$\ln C_t/C_o$	Standard Deviation
		Exp - 1	Exp - 2	Exp - 3						
TiO ₂	2	0.303	0.302	0.300	0.301	0.992	0.998	0.993	-0.007	± 0.001
	3	0.300	0.294	0.298	0.297	0.985		0.986	-0.014	± 0.003
	4	0.246	0.198	0.186	0.210	0.818		0.819	-0.199	± 0.031
	5	0.121	0.123	0.126	0.123	0.651		0.652	-0.427	± 0.002
N- TiO ₂	2	0.279	0.276	0.280	0.278	0.948	0.954	0.993	-0.007	± 0.002
	3	0.242	0.245	0.250	0.245	0.885		0.927	-0.075	± 0.004
	4	0.155	0.165	0.159	0.159	0.720		0.754	-0.282	± 0.005
	5	0.065	0.078	0.080	0.074	0.557		0.583	-0.539	± 0.008
0.1% Cu-NT	2	0.271	0.270	0.275	0.272	0.937	0.945	0.992	-0.009	± 0.002
	3	0.216	0.220	0.230	0.222	0.841		0.889	-0.117	± 0.007
	4	0.139	0.136	0.124	0.133	0.670		0.708	-0.345	± 0.007
	5	0.053	0.060	0.058	0.057	0.525		0.555	-0.588	± 0.003
0.5% Cu-NT	2	0.275	0.273	0.270	0.272	0.937	0.943	0.990	-0.007	± 0.002
	3	0.214	0.213	0.216	0.214	0.826		0.875	-0.133	± 0.001
	4	0.124	0.128	0.139	0.130	0.665		0.705	-0.349	± 0.007
	5	0.027	0.025	0.023	0.025	0.463		0.495	-0.713	± 0.002
1% Cu-NT	2	0.271	0.268	0.267	0.268	0.929	0.938	0.990	-0.010	± 0.002
	3	0.201	0.203	0.201	0.201	0.801		0.853	-0.159	± 0.001
	4	0.124	0.125	0.130	0.126	0.657		0.700	-0.356	± 0.003
	5	0.021	0.023	0.029	0.024	0.462		0.482	-0.729	± 0.004
2% Cu-NT	2	0.196	0.199	0.192	0.195	0.789	0.920	0.857	-0.154	± 0.003
	3	0.145	0.146	0.142	0.144	0.692		0.752	-0.285	± 0.002
	4	0.039	0.038	0.036	0.037	0.486		0.528	-0.638	± 0.001
	5	0.019	0.020	0.016	0.018	0.289		0.314	-1.158	± 0.002
3% Cu-NT	2	0.198	0.201	0.194	0.197	0.793	0.930	0.852	-0.160	± 0.003
	3	0.168	0.170	0.162	0.166	0.734		0.789	-0.236	± 0.004
	4	0.064	0.062	0.060	0.062	0.534		0.574	-0.555	± 0.002
	5	0.023	0.024	0.022	0.023	0.315		0.338	-1.084	± 0.001

Table 4.6 shows the calculations done for the application of all the prepared catalyst against methyl orange degradation.

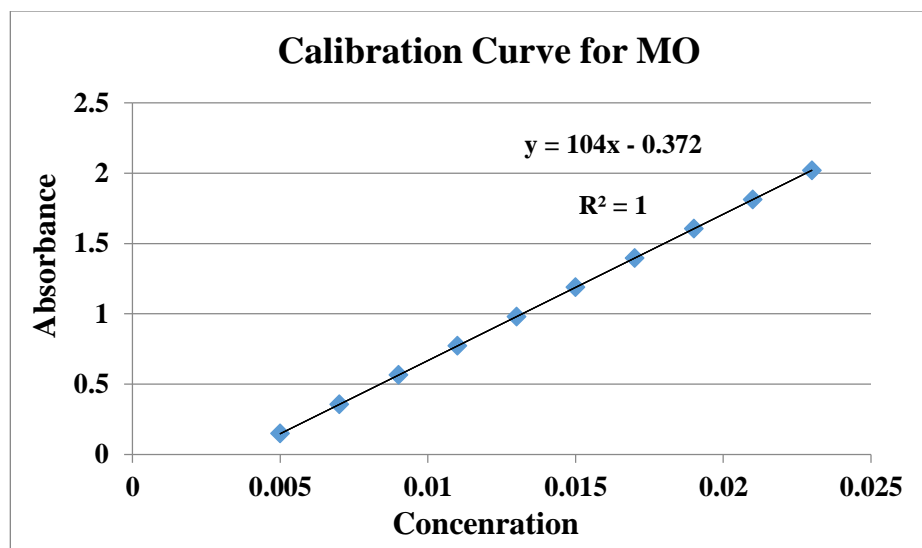


Figure 4.11 Plot between $\ln C_0/C_t$ vs time for MO

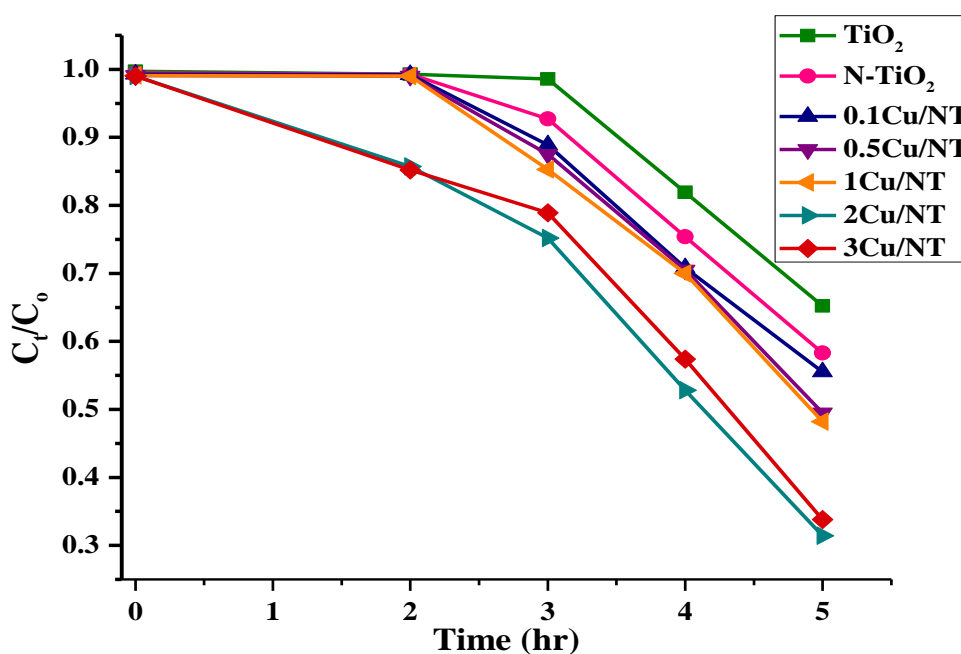


Figure 4.12 Activity of all prepared nanoparticles against methyl orange degradation

The linearity of a graph in **figure 4.11** shows the order of reaction is first order under pseudo condition. From the slope rate constant can be calculated.

Figure 4.12 shows the activity of all the prepared catalysts against degradation of methyl orange with the passage of time in terms of C_t/C_0 . It can be seen that 2% Cu/N co-doped

TiO₂ nanoparticles show best efficiency against MO degradation and 3% Cu/N co-doped TiO₂ nanoparticles show decreased efficiency.

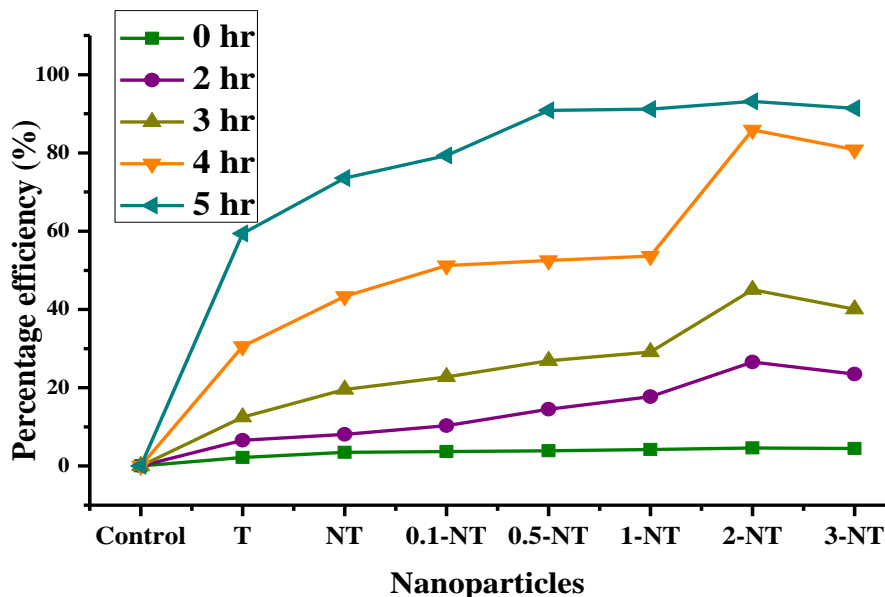


Figure 4.13 Efficiency of all prepared nanoparticles against degradation of MO

Figure 4.13 shows the efficiency of all the prepared catalysts against MO degradation in percentage. It can be seen that 2% Cu/N co-doped TiO₂ shows best percentage efficiency than all the other catalysts.

It was perfectly clear from all the evidences that 2% Cu/N co-doped TiO₂ nanoparticles showed better efficiency of 93% in terms of degradation of MO than all other catalysts. The next step was to produce the nanocomposites based on GO and the best efficient catalyst with varying ratios of GO (0.5, 1, 2) and study their degradation rates on MO similarly. Same method was taken, 50 mg of the prepared composites was taken separately with 0.01 mM of MO in a 50 ml volumetric flask and the solution was kept in dark for 2 hours to attain adsorption-desorption equilibrium. This solution from dark was then removed and placed under visible light in a photocatalytic chamber. As the reaction rate was fast, 5 ml of solution was taken from each solution after every 15 minute, which was then centrifuged for 3 min at 10000 rpm and the UV-Vis spectrophotometer was again used to study the degradation rate.

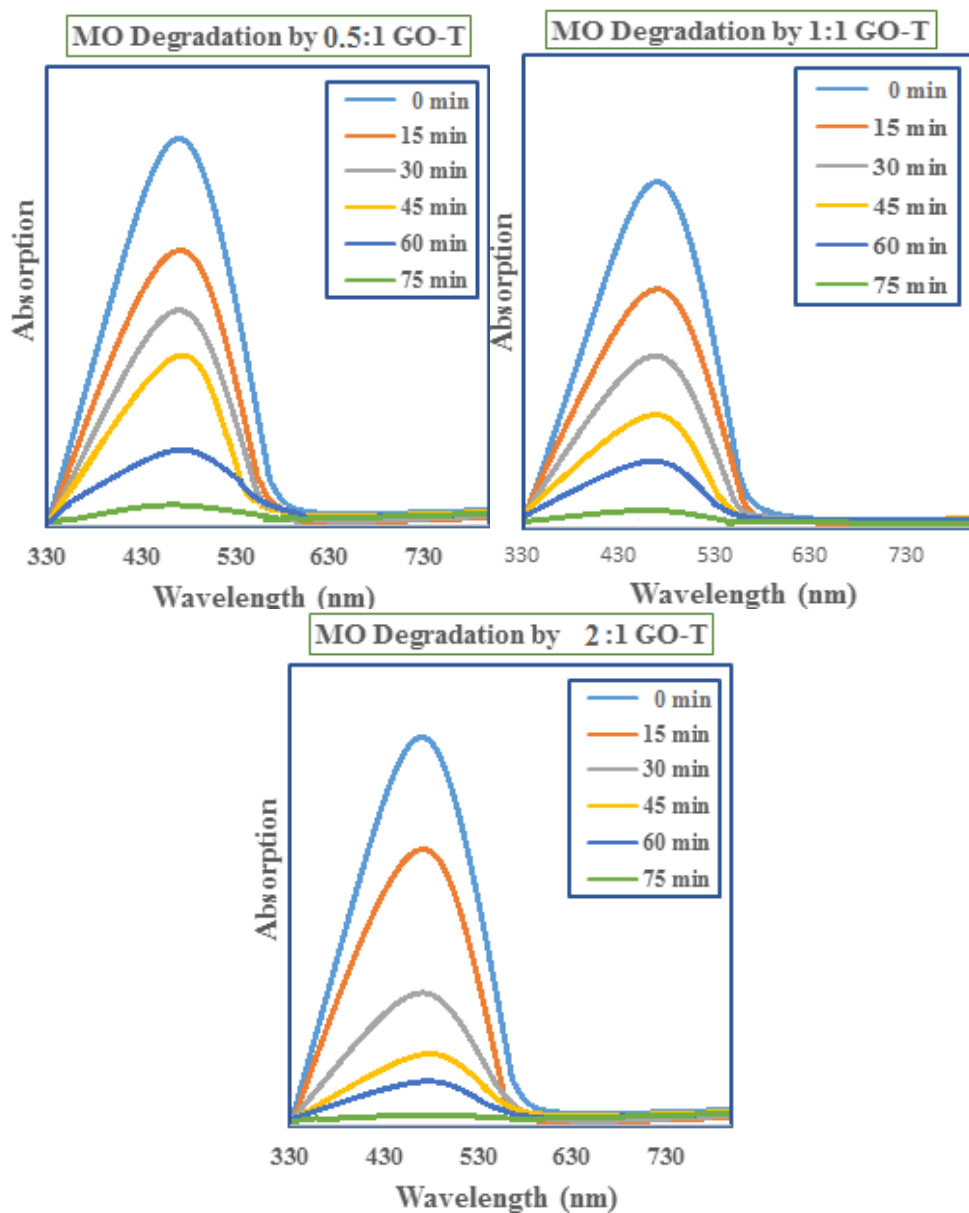


Figure 4.14 Degradation spectra of methyl orange using all prepared nanocomposites

All the spectra in **figure 4.14** show the degradation of methyl orange when nanocomposites were used. It can be seen that the highest concentration of GO based composite shows the highest efficiency against MO degradation. The overall degradation was done in 75 minutes total.

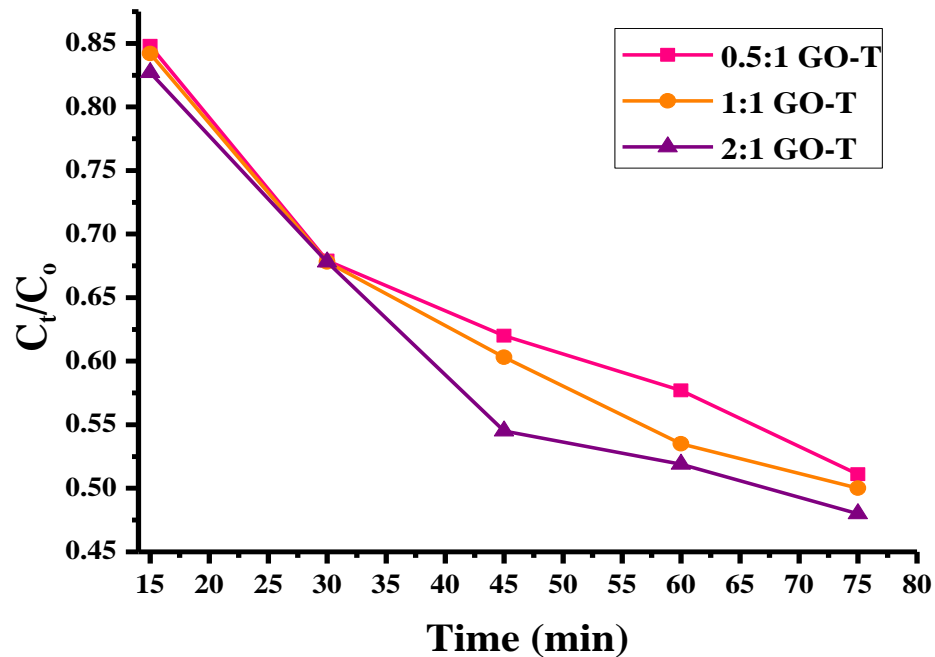


Figure 4.15 Activity of all prepared nanocomposites against Methyl Orange degradation

The comparison of their degradation rates is shown in **figure 4.15** and it is clear there that 2:1 GO: 2% Cu/N co-doped TiO₂ is showing the highest degradation efficiency.

Moreover, this degradation rate is also compared for each composite in the manner of percentage efficiency and is shown in **figure 4.16**. The highest obtained efficiency is for 2:1 GO-T which is 96%.

The formula used for the calculation of percentage efficiency is:

$$\text{Percentage Efficiency} = \left\{ \frac{(A_0 - A_t)}{A_0} \right\} \times 100$$

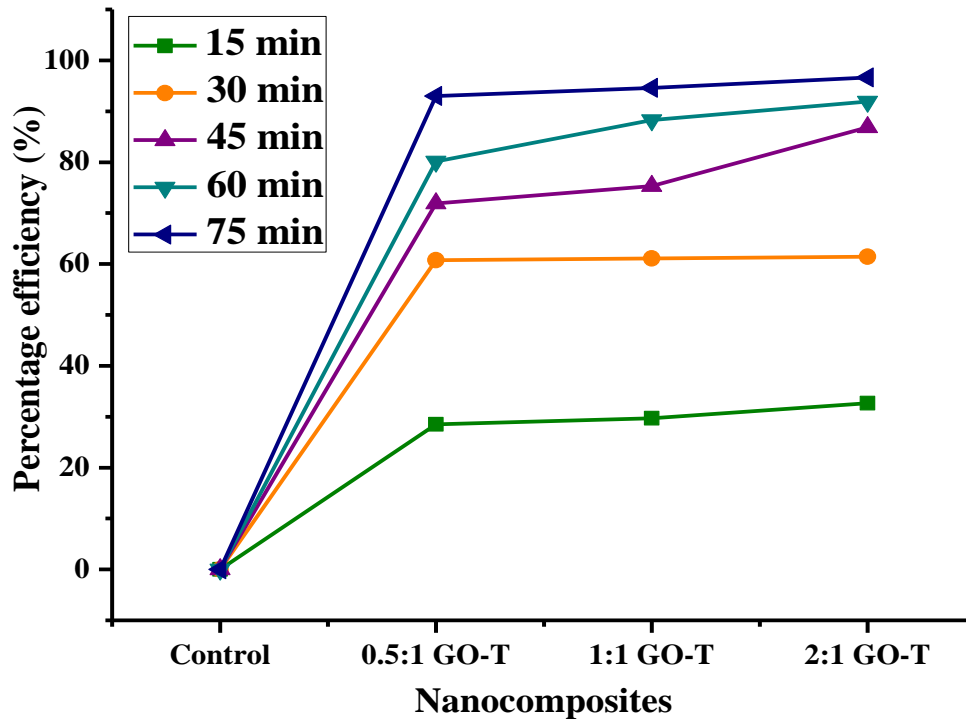


Figure 4.16 Efficiency of all prepared nanocomposites against degradation of MO

Table 4.7 shows all the calculations based on the degradation study of MO using all the prepared composites. After all the calculated results and graphs obtained by the studies, it was confirmed that 2% Cu/N co-doped TiO₂ is proven to be the best catalyst and the best nanocomposite is proven to be 2:1 GO- 2% Cu/N co-doped TiO₂.

The average of total three readings for each sample was taken after every 15 minutes and for total 75 minutes and their calculations were done. The standard deviation is shown in the table and it is clear that there is slight difference in all the three readings for each 15 minute. Also from the table the absorption values clearly illustrate 2:1 GO-T to be the best nanocomposite for the degradation of methyl orange.

Table 4.7 Degradation rate calculations for MO degradation using all composites under visible light irradiation

Catalyst	Time (min)	Absorbance			Average	C_t	C_0	C_t/C_0	$\ln C_t/C_0$	Standard Deviation
		Exp - 1	Exp - 2	Exp - 3						
0.5:1 GO-T	15	0.170	0.174	0.176	0.173	0.747	0.880	0.848	-0.164	± 0.003
	30	0.098	0.090	0.097	0.095	0.598		0.679	-0.387	± 0.004
	45	0.067	0.070	0.068	0.068	0.546		0.620	-0.478	± 0.001
	60	0.048	0.050	0.046	0.048	0.508		0.577	-0.549	± 0.002
	75	0.017	0.016	0.019	0.017	0.448		0.509	-0.675	± 0.001
1:1 GO-T	15	0.169	0.170	0.167	0.168	0.738	0.876	0.842	-0.171	± 0.001
	30	0.094	0.098	0.089	0.093	0.594		0.678	-0.338	± 0.004
	45	0.062	0.058	0.059	0.059	0.529		0.603	-0.505	± 0.002
	60	0.026	0.028	0.030	0.028	0.469		0.535	-0.625	± 0.002
	75	0.014	0.013	0.012	0.013	0.440		0.502	-0.689	± 0.001
2:1 GO-T	15	0.155	0.160	0.162	0.159	0.720	0.870	0.827	-0.189	± 0.003
	30	0.089	0.093	0.091	0.091	0.590		0.678	-0.388	± 0.002
	45	0.032	0.035	0.028	0.031	0.475		0.545	-0.606	± 0.003
	60	0.019	0.018	0.020	0.019	0.452		0.519	-0.655	± 0.001
	75	0.008	0.010	0.007	0.008	0.431		0.495	-0.703	± 0.001

5 CONCLUSION

Copper and nitrogen co-doped TiO₂ samples were synthesized using simple sol-gel method. Concentrations for copper were varied from 0.1% to 3% where, concentration of nitrogen was kept constant. Samples were characterized to check their optical and morphological properties. XRD data interpretation showed the crystallite size between 20-14 nm and SEM data showed the average particle size between 36-17 nm. The maximum particle and crystallite size was for pure TiO₂ and least particle and crystallite size was for highest doped TiO₂. SEM also showed the spherical morphology of all the nanoparticles but increased agglomeration was observed for increased Cu concentration. Band gap of prepared samples was decreased from 3.21 to 2.36 eV. Degradation studies against methyl orange were done and the best catalyst was 2% Cu/N co-doped TiO₂ nanoparticles with efficiency up to 93%. To further improve its properties, GO was incorporated in the best doped catalyst and it further reduced the bandgap to 2.09 eV for the highest amount of GO based TiO₂ nanocomposite. For GO-T composites, degradation studies were again performed against methyl orange to check their efficiency. The efficiency increased to 96% for 2:1 GO-T which was the highest concentration of GO based composite. In future, all of these prepared catalysts can be used for the degradation studies of many other organophosphates, pesticides and dyes and their efficiency can be measured.

6 REFERENCES

- [1] Dellamatrice, P. M., Silva-Stenico, M. E., de Moraes, L. A. B., Fiore, M. F., & Monteiro, R. T. R. (2017). Degradation of textile dyes by cyanobacteria. *Brazilian Journal of Microbiology*, 48(1), 25-31.
- [2] Sen, S. K., Raut, S., Bandyopadhyay, P., & Raut, S. (2016). Fungal discoloration and degradation of azo dyes: a review. *Fungal Biology Reviews*, 30(3), 112-133.
- [3] Konstantinou, I. K., & Albanis, T. A. (2004). TiO₂-assisted photocatalytic degradation of azo dyes in aqueous solution: kinetic and mechanistic investigations: a review. *Applied Catalysis B: Environmental*, 49(1), 1-14.
- [4] Mahmoodi, N. M., Keshavarzi, S., & Ghezelbash, M. (2017). Synthesis of nanoparticle and modelling of its photocatalytic dye degradation ability from colored wastewater. *Journal of Environmental Chemical Engineering*, 5(4), 3684-3689.
- [5] Charanpahari, A., Umare, S. S., Gokhale, S. P., Sudarsan, V., Sreedhar, B., & Sasikala, R. (2012). Enhanced photocatalytic activity of multi-doped TiO₂ for the degradation of methyl orange. *Applied Catalysis A: General*, 443, 96-102.
- [6] Vautier, M., Guillard, C., & Herrmann, J. M. (2001). Photocatalytic degradation of dyes in water: case study of indigo and of indigo carmine. *Journal of Catalysis*, 201(1), 46-59.
- [7] Akpan, U. G., & Hameed, B. H. (2009). Parameters affecting the photocatalytic degradation of dyes using TiO₂-based photocatalysts: a review. *Journal of Hazardous Materials*, 170(2), 520-529.
- [8] Pascual, J., Camassel, J., & Mathieu, H. (1977). Resolved Quadrupolar Transition in TiO₂. *Physical Review Letters*, 39(23), 1490.
- [9] Wold, A. (1993). Photocatalytic properties of titanium dioxide (TiO₂). *Chemistry of Materials*, 5(3), 280-283.
- [10] Hashimoto, K., Irie, H., & Fujishima, A. (2005). TiO₂ photocatalysis: a historical overview and future prospects. *Japanese Journal of Applied Physics*, 44(12R), 8269.

-
- [11] Saggiaro, E. M., Oliveira, A. S., Pavesi, T., Maia, C. G., Ferreira, L. F. V., & Moreira, J. C. (2011). Use of titanium dioxide photocatalysis on the remediation of model textile wastewaters containing azo dyes. *Molecules*, *16*(12), 10370-10386.
- [12] Ni, M., Leung, M. K., Leung, D. Y., & Sumathy, K. (2007). A review and recent developments in photocatalytic water-splitting using TiO₂ for hydrogen production. *Renewable and Sustainable Energy Reviews*, *11*(3), 401-425.
- [13] Zaleska, A. (2008). Doped-TiO₂: a review. *Recent Patents on Engineering*, *2*(3), 157-164.
- [14] Ni, M., Leung, M. K., Leung, D. Y., & Sumathy, K. (2007). A review and recent developments in photocatalytic water-splitting using TiO₂ for hydrogen production. *Renewable and Sustainable Energy Reviews*, *11*(3), 401-425.
- [15] Janisch, R., Gopal, P., & Spaldin, N. A. (2005). Transition metal-doped TiO₂ and ZnO—present status of the field. *Journal of Physics: Condensed Matter*, *17*(27), R657.
- [16] Pongwan, P., Wetchakun, K., Phanichphant, S., & Wetchakun, N. (2016). Enhancement of visible-light photocatalytic activity of Cu-doped TiO₂ nanoparticles. *Research on Chemical Intermediates*, *42*(4), 2815-2830.
- [17] Pongwan, P., Wetchakun, K., Phanichphant, S., & Wetchakun, N. (2016). Enhancement of visible-light photocatalytic activity of Cu-doped TiO₂ nanoparticles. *Research on Chemical Intermediates*, *42*(4), 2815-2830.
- [18] Yalçın, Y., Kılıç, M., & Çınar, Z. (2010). The role of non-metal doping in TiO₂ photocatalysis. *Journal of Advanced Oxidation Technologies*, *13*(3), 281-296.
- [19] Umabayashi, T., Yamaki, T., Itoh, H., & Asai, K. (2002). Band gap narrowing of titanium dioxide by sulfur doping. *Applied Physics Letters*, *81*(3), 454-456.
- [20] Bingham, S., & Daoud, W. A. (2011). Recent advances in making nano-sized TiO₂ visible-light active through rare-earth metal doping. *Journal of Materials Chemistry*, *21*(7), 2041-2050.
- [21] Thompson, T. L., & Yates, J. T. (2005). TiO₂-based photocatalysis: surface defects, oxygen and charge transfer. *Topics in Catalysis*, *35*(3), 197-210.

-
- [22] Chen, X., &Burda, C. (2008). The electronic origin of the visible-light absorption properties of C-, N-and S-doped TiO₂ nanomaterials. *Journal of the American Chemical Society*, 130(15), 5018-5019.
- [23] Katsnelson, M. I. (2007). Graphene: carbon in two dimensions. *Materials Today*, 10(1), 20-27.
- [24] Xiang, Q., Yu, J., &Jaroniec, M. (2012). Graphene-based semiconductor photocatalysts. *Chemical Society Reviews*, 41(2), 782-796.
- [25] Geim, A. K., &Novoselov, K. S. (2007). The rise of graphene. *Nature Materials*, 6(3), 183-191.
- [26] Eda, G., &Chhowalla, M. (2010). Chemically derived graphene oxide: towards large-area thin-film electronics and optoelectronics. *Advanced Materials*, 22(22), 2392-2415.
- [27] Štengl, V., Bakardjieva, S., Grygar, T. M., Bludská, J., &Kormunda, M. (2013). TiO₂-graphene oxide nanocomposite as advanced photocatalytic materials. *Chemistry Central Journal*, 7(1), 41.
- [28] Minella, M., Sordello, F., &Minero, C. (2017). Photocatalytic process in TiO₂/graphene hybrid materials. Evidence of charge separation by electron transfer from reduced graphene oxide to TiO₂. *Catalysis Today*, 281, 29-37.
- [29] Chen, C., Cai, W., Long, M., Zhou, B., Wu, Y., Wu, D., & Feng, Y. (2010). Synthesis of visible-light responsive graphene oxide/TiO₂ composites with p/nheterojunction. *Acs Nano*, 4(11), 6425-6432.
- [30] MalekshahiByranvand, M., NematiKharat, A., Fatholahi, L., &MalekshahiBeiranvand, Z. (2013). A review on synthesis of nano-TiO₂ via different methods. *Journal of Nanostructures*, 3(1), 1-9.
- [31] Jagadale, T. C., Takale, S. P., Sonawane, R. S., Joshi, H. M., Patil, S. I., Kale, B. B., &Ogale, S. B. (2008). N-doped TiO₂ nanoparticle based visible light photocatalyst by modified peroxide sol– gel method. *The Journal of Physical Chemistry C*, 112(37), 14595-14602.
- [32] Sun, X., Zheng, C., Zhang, F., Yang, Y., Wu, G., Yu, A., & Guan, N. (2009). Size-controlled synthesis of magnetite (Fe₃O₄) nanoparticles coated with glucose and

-
- gluconic acid from a single Fe (III) precursor by a sucrose bi-functional hydrothermal method. *The Journal of Physical Chemistry C*, 113(36), 16002-16008.
- [33] Li, B., Xie, Y., Huang, J., & Qian, Y. (1999). Synthesis by a solvothermal route and characterization of CuInSe₂ nanowhiskers and nanoparticles. *Advanced Materials*, 11(17), 1456-1459.
- [34] Swihart, M. T. (2003). Vapor-phase synthesis of nanoparticles. *Current Opinion in Colloid & Interface Science*, 8(1), 127-133.
- [35] Gerbec, J. A., Magana, D., Washington, A., & Strouse, G. F. (2005). Microwave-enhanced reaction rates for nanoparticle synthesis. *Journal of the American Chemical Society*, 127(45), 15791-15800.
- [36] Zhu, S., Zhou, H., Hibino, M., Honma, I., & Ichihara, M. (2005). Synthesis of MnO₂ nanoparticles confined in ordered mesoporous carbon using a sonochemical method. *Advanced Functional Materials*, 15(3), 381-386.
- [37] Cai, M., Thorpe, D., Adamson, D. H., & Schniepp, H. C. (2012). Methods of graphite exfoliation. *Journal of Materials Chemistry*, 22(48), 24992-25002.
- [38] Paulchamy, B., Arthi, G., & Lignesh, B. D. (2015). A simple approach to stepwise synthesis of graphene oxide nanomaterial. *Journal of Nano medicine & Nanotechnology*, 6(1), 1.
- [39] Teo, P. S., Lim, H. N., Huang, N. M., Chia, C. H., & Harrison, I. (2012). Room temperature in situ chemical synthesis of Fe₃O₄/graphene. *Ceramics International*, 38(8), 6411-6416.
- [40] Lu, T., Pan, L., Li, H., Zhu, G., Lv, T., Liu, X., Chua, D. H. (2011). Microwave-assisted synthesis of graphene-ZnO nanocomposite for electrochemical super capacitors. *Journal of Alloys and Compounds*, 509(18), 5488-5492.
- [41] Mai, Y. J., Wang, X. L., Xiang, J. Y., Qiao, Y. Q., Zhang, D., Gu, C. D., & Tu, J. P. (2011). CuO/graphene composite as anode materials for lithium-ion batteries. *Electrochimica Acta*, 56(5), 2306-2311.
- [42] Li, B., & Cao, H. (2011). ZnO@ graphene composite with enhanced performance for the removal of dye from water. *Journal of Materials Chemistry*, 21(10), 3346-3349.

-
- [43] Zhang, M., Lei, D., Du, Z., Yin, X., Chen, L., Li, Q., Wang, T. (2011). Fast synthesis of SnO₂/graphene composites by reducing graphene oxide with stannous ions. *Journal of Materials Chemistry*, 21(6), 1673-1676.
- [44] Xu, X. R., Li, H. B., Wang, W. H., & Gu, J. D. (2004). Degradation of dyes in aqueous solutions by the Fenton process. *Chemosphere*, 57(7), 595-600.
- [45] Pauling, L. (1939). A Theory of the Color of Dyes. *Proceedings of the National Academy of Sciences*, 25(11), 577-582.
- [46] Konstantinou, I. K., & Albanis, T. A. (2004). TiO₂-assisted photocatalytic degradation of azo dyes in aqueous solution: kinetic and mechanistic investigations: a review. *Applied Catalysis B: Environmental*, 49(1), 1-14.
- [47] Sandberg, R. G., Henderson, G. H., White, R. D., & Eyring, E. M. (1972). Kinetics of acid dissociation-ion recombination of aqueous methyl orange. *The Journal of Physical Chemistry*, 76(26), 4023-4025.
- [48] Ajmal, A., Majeed, I., Malik, R. N., Idriss, H., & Nadeem, M. A. (2014). Principles and mechanisms of photocatalytic dye degradation on TiO₂ based photocatalysts: a comparative overview. *Rsc Advances*, 4(70), 37003-37026.
- [49] Fujishima, A., & Honda, K. (1972). Electrochemical photolysis of water at a semiconductor electrode. *Nature*, 238(5358), 37-38.
- [50] Han, H., & Bai, R. (2009). Buoyant photocatalyst with greatly enhanced visible-light activity prepared through a low temperature hydrothermal method. *Industrial & Engineering Chemistry Research*, 48(6), 2891-2898.
- [51] Frank, S. N., & Bard, A. J. (1977). Heterogeneous photocatalytic oxidation of cyanide ion in aqueous solutions at titanium dioxide powder. *Journal of the American Chemical Society*, 99(1), 303-304.
- [52] Wang, C. C., & Ying, J. Y. (1999). Sol-gel synthesis and hydrothermal processing of anatase and rutile Titania nanocrystals. *Chemistry of Materials*, 11(11), 3113-3120.
- [53] Yang, H., Zhang, K., Shi, R., Li, X., Dong, X., & Yu, Y. (2006). Sol-gel synthesis of TiO₂ nanoparticles and photocatalytic degradation of methyl orange in aqueous TiO₂ suspensions. *Journal of Alloys and Compounds*, 413(1), 302-306.

-
- [54] Hamadani, M., Reisi-Vanani, A., &Majedi, A. (2010). Sol-gel preparation and characterization of Co/TiO₂ nanoparticles: application to the degradation of methyl orange. *Journal of the Iranian Chemical Society*, 7(1), S52-S58.
- [55] Vijayalakshmi, R., &Rajendran, V. (2012). Synthesis and characterization of nano-TiO₂ via different methods. *Arch App Sci Res*, 4(2), 1183-1190.
- [56] Sharma, A., Karn, R. K., &Pandiyan, S. K. (2014). Synthesis of TiO₂ Nanoparticles by Sol-gel Method and Their Characterization. *J. Basic Appl. Eng. Res.*, 1, 1-5.
- [57] Sabry, R. S., Al-Haidarie, Y. K., &Kudhier, M. A. (2016). Synthesis and photocatalytic activity of TiO₂ nanoparticles prepared by sol–gel method. *Journal of Sol-Gel Science and Technology*, 78(2), 299-306.
- [58] Sathish, M., Viswanathan, B., Viswanath, R. P., &Gopinath, C. S. (2005). Synthesis, characterization, electronic structure, and photocatalytic activity of nitrogen-doped TiO₂ nanocatalyst. *Chemistry of materials*, 17(25), 6349-6353.
- [59] Huang, Y. U., Zheng, X., Zhongyi, Y. I. N., Feng, T. A. G., Beibei, F. A. N. G., &Keshan, H. O. U. (2007). Preparation of Nitrogen-doped TiO₂ Nanoparticle Catalyst and Its Catalytic Activity under Visible Light** Supported by the Science and Technology Research Program of Chongqing Education Commission (KJ050702), and the Natural Science Foundation Project of Chongqing Science and Technology Commission (No. 2007BB7208). *Chinese Journal of Chemical Engineering*, 15(6), 802-807.
- [60] Senthilnathan, J., & Philip, L. (2010). Photocatalytic degradation of lindane under UV and visible light using N-doped TiO₂. *Chemical Engineering Journal*, 161(1), 83-92.
- [61] Hassanvand, A., Sohrabi, M., Royae, S. J., & Jafarikajour, M. (2014). Preparation and characterization of nitrogen doped TiO₂ nanoparticles as an effective catalyst in photodegradation of phenol under visible light. In *Advanced Materials Research* (Vol. 875, pp. 28-33). Trans Tech Publications.
- [62] Abdullah, A. M., Al-Thani, N. J., Tawbi, K., & Al-Kandari, H. (2016). Carbon/nitrogen-doped TiO₂: new synthesis route, characterization and application for phenol degradation. *Arabian Journal of Chemistry*, 9(2), 229-237.

-
- [63] Song, K., Zhou, J., Bao, J., & Feng, Y. (2008). Photocatalytic activity of (copper, nitrogen) -co-doped titanium dioxide nanoparticles. *Journal of the American Ceramic Society*, 91(4), 1369-1371.
- [64] López, R., Gómez, R., & Llanos, M. E. (2009). Photophysical and photocatalytic properties of nano-sized copper-doped Titania sol-gel catalysts. *Catalysis Today*, 148(1), 103-108.
- [65] Jaiswal, R., Bharambe, J., Patel, N., Dashora, A., Kothari, D. C., & Miotello, A. (2015). Copper and Nitrogen co-doped TiO₂ photocatalyst with enhanced optical absorption and catalytic activity. *Applied Catalysis B: Environmental*, 168, 333-341.
- [66] Pongwan, P., Wetchakun, K., Phanichphant, S., & Wetchakun, N. (2016). Enhancement of visible-light photocatalytic activity of Cu-doped TiO₂ nanoparticles. *Research on Chemical Intermediates*, 42(4), 2815-2830.
- [67] Reda, S. M., Khairy, M., & Mousa, M. A. (2017). Photocatalytic activity of nitrogen and copper doped TiO₂ nanoparticles prepared by microwave-assisted sol-gel process. *Arabian Journal of Chemistry*.
- [68] Krishnamoorthy, K., Mohan, R., & Kim, S. J. (2011). Graphene oxide as a photocatalytic material. *Applied Physics Letters*, 98(24), 244101.
- [69] Hummers Jr, W. S., & Offeman, R. E. (1958). Preparation of graphitic oxide. *Journal of the American Chemical Society*, 80(6), 1339-1339.
- [70] Chen, J., Yao, B., Li, C., & Shi, G. (2013). An improved Hummers method for eco-friendly synthesis of graphene oxide. *Carbon*, 64, 225-229.
- [71] Shahriary, L., & Athawale, A. A. (2014). Graphene oxide synthesized by using modified hummers approach. *Int. J. Renew. Energy Environ. Eng*, 2(01), 58-63.
- [72] Paulchamy, B., Arthi, G., & Lignesh, B. D. (2015). A simple approach to stepwise synthesis of graphene oxide nanomaterial. *Journal of Nanomedicine & Nanotechnology*, 6(1), 1.
- [73] Khalid, N. R., Ahmed, E., Hong, Z., Zhang, Y., & Ahmad, M. (2012). Nitrogen doped TiO₂ nanoparticles decorated on graphene sheets for photocatalysis applications. *Current Applied Physics*, 12(6), 1485-1492.

-
- [74] Khalid, N. R., Ahmed, E., Hong, Z., Ahmad, M., Zhang, Y., & Khalid, S. (2013). Cu-doped TiO₂ nanoparticles/graphene composites for efficient visible-light photocatalysis. *Ceramics International*, 39(6), 7107-7113.
- [75] Shang, X., Zhang, M., Wang, X., & Yang, Y. (2014). Sulfur, nitrogen-doped TiO₂/graphene oxide composites as a high performance photocatalyst. *Journal of Experimental Nanoscience*, 9(7), 749-761.
- [76] Yadav, H. M., & Kim, J. S. (2016). Solvothermal synthesis of anatase TiO₂-graphene oxide nanocomposites and their photocatalytic performance. *Journal of Alloys and Compounds*, 688, 123-129.